



MOX–Report No. 32/2012

**A reduced model for Darcy's problem in networks of fractures**

FORMAGGIA, L.; FUMAGALLI, A.; SCOTTI A.; RUFFO, P

MOX, Dipartimento di Matematica "F. Brioschi"  
Politecnico di Milano, Via Bonardi 9 - 20133 Milano (Italy)

[mox@mate.polimi.it](mailto:mox@mate.polimi.it)

<http://mox.polimi.it>



# A reduced model for Darcy's problem in networks of fractures

Luca Formaggia<sup>‡</sup>      Alessio Fumagalli<sup>‡</sup>      Anna Scotti<sup>‡</sup>  
Paolo Ruffo<sup>†</sup>

August 14, 2012

<sup>‡</sup> MOX– Modellistica e Calcolo Scientifico  
Dipartimento di Matematica “F. Brioschi”  
Politecnico di Milano  
via Bonardi 9, 20133 Milano, Italy  
luca.formaggia@polimi.it  
alessio.fumagalli@mail.polimi.it  
anna.scotti@mail.polimi.it

<sup>†</sup> eni spa- exploration & production division  
5° Palazzo Uffici - Room 4046 E  
GEBA Dept.  
Via Emilia, 1, 20097 San Donato Milanese (MI), Italy  
paolo.ruffo@eni.com

**Keywords:** Reduced models, fractured porous media, XFEM.

**AMS Subject Classification:** 05A16, 65N38, 78M50

## Abstract

Subsurface flows are influenced by the presence of faults and large fractures which act as preferential paths or barriers for the flow. In literature models were proposed to handle fractures in a porous medium as objects of codimension 1. In this work we consider the case of a network of intersecting fractures, with the aim of deriving physically consistent and effective interface conditions to impose at the intersection between fractures. This new model accounts for the angle between fractures at the intersections and allows for jumps of pressure across the intersection. This latter property permits to describe more accurately the flow when fractures are characterised by different properties, than other models that impose pressure continuity. The main mathematical properties of the model, derived in the two-dimensional setting, are analysed. As concerns the numerical

discretization we allow the grids of the fractures to be independent, thus in general non-matching at the intersection, by means of the *extended finite element method* (XFEM), to increase the flexibility of the method in the case of complex geometries characterized by a high number of fractures.

## 1 Introduction

The presence of fractures can largely influence the flow in porous media in geophysical applications. In particular, large fractures and faults can act, according to their different permeabilities, as barriers of preferential paths to the flow. At a different space scale micro fractures can alter, according to their density and orientation, the overall permeability of the porous medium. Numerical simulations of problems related to groundwater flow such as  $CO_2$  storage, oil migration and recovery or groundwater contamination should be able to account for the presence of fractures to yield accurate results.

In the applications we are considering, the porous medium is usually characterized by the presence of several fractures that can intersect each other. Moreover the characteristic thickness, or aperture, of the fractures is very small compared to their length and, in particular, compared to the typical size of the domain of interest. This geometric complexity makes the simulations particularly challenging for standard methods.

In [2, 13, 15] the authors proposed a model reduction strategy to overcome part of the aforementioned problems by using a domain decomposition approach, where fractures are represented as natural one-codimension interfaces inside the porous domains. The proposed model can successfully reduce the number of unknowns in the simulation since, instead of refining the grid to capture a thin  $n$ -dimensional region we are replacing it with a  $n - 1$ -dimensional interface. This approach, originally developed for the single-phase Darcy problem has been successfully extended to passive transport in porous media [10] and to two-phase flow [14, 11], with suitable reduced models to describe the flow in the fracture. However the aforementioned works consider just the restricted case of non-intersecting fractures, that completely cut the domain into two separated sub-domains. In [4] this assumptions are relaxed to include fractures that do not cut entirely the domain, *i.e.* fractures with tips immersed in the enclosing porous medium, with the constraint of mesh conformity between the fractures and the porous medium.

Realistic simulations in a three dimensional domain are presented in [3], where suitable coupling conditions are imposed at the intersections between fractures. In particular, the continuity of pressure and mass conservation are enforced. These conditions however, also used in [2], may lead to inaccurate results if two intersecting fractures have different characteristics, in particular different permeabilities. In this case one may expect strong variations of pressure near the intersection, thus pressure continuity does not seem an appropriate condition to represent this behaviour in a model reduction approach.

In this work we focus on the development of a reduced model that generalizes the coupling conditions of [3, 2] to account for different properties of the fractures such as different permeabilities and thicknesses and to include the effect of the intersection angle. The new coupling conditions allow for pressure and velocity jumps at the intersection, similarly to the conditions derived in [15] for the matrix-fracture system. Hence, we account for the fact that in a fracture system one fracture can act as a barrier or a preferential path with respect to the other. We analyse the resulting coupled system of equations to derive its well posedness, and assess its conservation and positivity properties. Although the analysis is focused on the two dimensional case, where fractures are modelled as one dimensional manifolds. We propose a discretization method that allows for non matching grids at the intersection points with the intent of providing the maximal flexibility when dealing with complex networks. More precisely, we employ an extended finite element (XFEM) strategy to treat intersecting fractures.

We focus just on the fracture network neglecting the flow in the surrounding medium. This choice can be regarded as an intermediate step for the development of the fully coupled model with intersecting fractures immersed in a permeable medium, but also as a reasonable approximation of realistic situations where the rock has low permeability and the flow occurs mainly through the fracture network.

The paper is structured as follows. In Section 2 we introduce the governing equations and provide the setting for the derivation of the reduced model. In Section 3 the reduced model for the intersecting fractures is derived. The corresponding weak formulation in mixed form and its analysis is presented in Section 4, while in Section 5 we address the numerical discretization. In Section 6 we present some numerical test cases to assess the theoretical properties of the model and the discretization method. Finally, Section 7 is devoted to conclusions.

## 2 The governing equations

For the sake of simplicity, let us consider two intersecting fractures  $\Omega_1, \Omega_2 \in \mathbb{R}^n$ , included in a domain of interest  $D \subset \mathbb{R}^n$ . The results illustrated in this section may be extended rather easily to the case of several fractures, as the examples in section 6 show. Furthermore, here we consider the case  $n = 2$ .

Following [15] we suppose that, for each  $\Omega_i$ , there exists a non auto-intersecting one dimensional manifold  $\gamma_i$  of class  $C^2$  such that  $\Omega_i$  may be defined as

$$\Omega_i = \left\{ \mathbf{x} \in \mathbb{R}^n : \mathbf{x} = \mathbf{s} + r\mathbf{n}_i, \mathbf{s} \in \gamma_i, r \in \left( -\frac{d_i(\mathbf{s})}{2}, \frac{d_i(\mathbf{s})}{2} \right) \right\}, \quad (1)$$

where  $d_i \in C^2(\gamma_i)$  is the thickness of  $\Omega_i$  and  $\mathbf{n}_i$  the unit normal of  $\gamma_i$ . If  $|\gamma_i|$  we assume that  $|\gamma_i| \gg d_i$ , for  $i = 1, 2$ . Furthermore, we assume that there exist

$c_1, c_2 \in \mathbb{R}^+$ , with  $c_2$  “small”, such that

$$d_i(\mathbf{s}) > c_1, \quad |d'_i(\mathbf{s})| < c_2 \quad \forall \mathbf{s} \in \gamma_i \quad \text{for } i = 1, 2.$$

In other words, we assume that the thickness of the fracture varies slowly and is small compared to the other dimensions of the fracture.

**Remark 1** *The requirement that  $\gamma_i$  be of class  $C^2$  may be partially dispensed with. Indeed, it is sufficient that  $\gamma_i$  be a piecewise  $C^2$  curve.*

We set  $I := \Omega_1 \cap \Omega_2$ . We assume that each  $\Omega_i$  can be subdivided into three disjoint and non-empty sub-regions  $\Omega_{i1}, \Omega_{i2}$  and  $I$ , *i.e.* a T shaped intersection is not allowed. For convenience let us introduce the following sets, for  $i, j = 1, 2$

$$\bar{\Omega} := \bar{\Omega}_1 \cup \bar{\Omega}_2, \quad \bar{\gamma} := \bar{\gamma}_1 \cup \bar{\gamma}_2, \quad \mathbf{i}_p := \gamma_1 \cap \gamma_2 \quad \text{and} \quad \partial I_{ij} := \partial I \cap \partial \Omega_{ij}. \quad (2)$$

It is implicit in this definitions that we assume that  $\gamma_1$  and  $\gamma_2$  intersect each other at a single point, indicated with  $\mathbf{i}_p$ . The extension to multiple intersection is however straightforward, see Figure 1 for a more general case of multiples fractures in two dimensions.

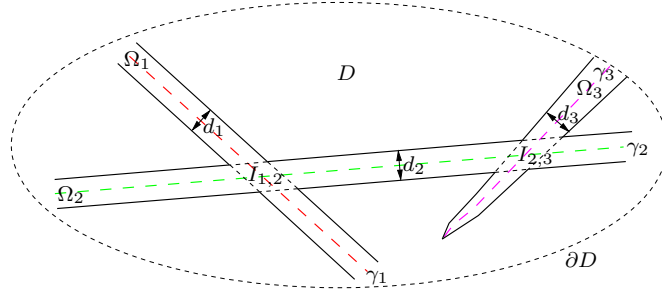


Figure 1: Example of a network of fractures and its subdivision (2).

We assume a Lipschitz-continuous boundary for both  $D$  and  $\Omega$ . We indicate with  $\mathbf{n}_{ij}, \mathbf{n}_\Omega$  and  $\mathbf{n}_D$  the outward unit normals to  $\partial I_{ij}, \partial \Omega$  and  $\partial D$ , respectively. Here and in the sequel we indicate with the lower case subscripts  $i$  and  $ij$  the restriction of data and unknowns to  $\Omega_i$  or  $\Omega_{ij}$ , respectively, and with the subscript  $I$  the restriction to  $I$ . For instance, for  $\mathbf{u}_i$  in  $\Omega_i$ ,  $\mathbf{u}_{ij}$  indicates the function in  $\Omega_{ij}$  such that  $\mathbf{u}_{ij} = \mathbf{u}_i|_{\Omega_{ij}}$  and so on. We are interested in computing the steady pressure field  $p$  and the velocity field  $\mathbf{u}$  in the whole network  $\Omega$ , which are governed by the Darcy problem formulated in  $\Omega_i$  and  $I$  as

$$\begin{cases} \nabla \cdot \mathbf{u}_i = f_i \\ \mathbf{K}_i^{-1} \mathbf{u}_i + \nabla p_i = \mathbf{0} \end{cases} \quad \text{in } \Omega_i \text{ for } i = 1, 2, \quad \begin{cases} \nabla \cdot \mathbf{u}_I = f_I \\ \mathbf{K}_I^{-1} \mathbf{u}_I + \nabla p_I = \mathbf{0} \end{cases} \quad \text{in } I. \quad (3)$$

Here  $\mathbf{K}_i \in [L^\infty(\Omega)]^{n \times n}$  and  $\mathbf{K}_I \in [L^\infty(\Omega)]^{n \times n}$  denote the permeability tensors, which are symmetric and positive definite, and  $f \in L^2(\Omega)$  is a source term which represents a possible mass source.

We consider the following physical coupling conditions between  $I$  and  $\Omega \setminus I$

$$\begin{cases} p_{ij} = p_I \\ \mathbf{u}_{ij} \cdot \mathbf{n}_{ij} = \mathbf{u}_I \cdot \mathbf{n}_{ij} \end{cases} \quad \text{on } \partial I_{ij} \text{ for } i, j = 1, 2, \quad (4)$$

and the boundary conditions

$$\begin{cases} \mathbf{u} \cdot \mathbf{n}_\Omega = 0 & \text{on } \partial\Omega \setminus \partial D, \\ p = g & \text{on } \Gamma^p, \\ \mathbf{u} \cdot \mathbf{n}_D = b & \text{on } \Gamma^u. \end{cases} \quad (5)$$

The first condition of (5) means that we are considering the fractures as immersed in an impermeable medium  $D \setminus \Omega$ . In the remaining part of  $\partial\Omega$  we impose boundary condition for the pressure on  $\Gamma^p$  with  $g \in H^{1/2}(\Gamma^p)$ , or for the flux on  $\Gamma^u$  with  $b \in H^{-1/2}(\Gamma^u)$ . Moreover we require that  $\Gamma^p \neq \emptyset$  and that  $\partial\Omega_{ij} \cap \partial D$  belongs to  $\Gamma^p$  or  $\Gamma^u$  for  $i, j = 1, 2$ . Introducing the vector functional space

$$\mathcal{H}_{\text{div}}(\Omega) := \{ \mathbf{v} \in \mathbf{H}_{\text{div}}(\Omega) : \langle \mathbf{v} \cdot \mathbf{n}_D - b, w \rangle = 0, \forall w \in H_{0, \Gamma^u}^1(\Omega) \},$$

with  $H_{0, \Gamma^u}^1(\Omega) := \{ w \in H^1(\Omega) : w = 0 \text{ in } \Gamma^u \}$ , we have the following standard result for the Darcy problem, see [6, 16, 8].

**Theorem 2.1** *Under the given hypothesis of the data problem (3) coupled with (4) and (5) is well posed. In particular we have  $(\mathbf{u}, p) \in \mathcal{H}_{\text{div}}(\Omega) \times L^2(\Omega)$ .*

### 3 Derivation of a reduced model

The derivation of the reduced model follows the approach presented, in a different framework, in [15]. We start by introducing a reduced model for each  $\Omega_i$ , which approximates the fracture with the line  $\gamma_i$ .

We indicate the projection operators in the normal and tangential direction of  $\gamma_i$  as  $\mathbf{N}_i := \mathbf{n}_i \otimes \mathbf{n}_i$  and  $\mathbf{T}_i := \mathbf{I} - \mathbf{N}_i$  respectively, with  $\mathbf{I}$  the identity tensor. Given two regular functions  $g$  and  $\mathbf{q}$ , we define the tangential gradient and divergence for each  $\gamma_i$  as

$$\nabla_{\tau_i} g := \mathbf{T}_i \nabla g \quad \text{and} \quad \nabla_{\tau_i} \cdot \mathbf{q} := \mathbf{T}_i : \nabla \mathbf{q}, \quad (6)$$

respectively. We require that the permeability tensor  $\mathbf{K}_i$  in  $\Omega_i \setminus I$ ,  $i = 1, 2$ , can be written as  $\mathbf{K}_i = K_{i, \mathbf{n}} \mathbf{N}_i + K_{i, \tau} \mathbf{T}_i$ , with  $K_{i, \mathbf{n}}, K_{i, \tau} \in L^\infty(\Omega_{ij})$  and strictly positive. This is a reasonable request since we are assuming, in the two-dimensional case, that the permeability tensor is diagonal in a frame of reference that is aligned with the fracture. In the three dimensional case this assumption also implies that the permeability should be isotropic in the tangent plane of the fracture.

We indicate with the symbol  $\hat{\cdot}$  the reduced variables defined on  $\gamma_i$ . In particular, for any  $\mathbf{s}_i \in \gamma_i$ , we introduce the reduced pressure  $\hat{p}$  and velocity  $\hat{\mathbf{u}}$  as

$$\hat{\mathbf{u}}_i(\mathbf{s}_i) := \int_{-\frac{d_i}{2}}^{\frac{d_i}{2}} \mathbf{T}_i \mathbf{u}_i(\mathbf{s}_i + r \mathbf{n}_i) dr \quad \text{and} \quad \hat{p}_i(\mathbf{s}_i) := \frac{1}{d_i} \int_{-\frac{d_i}{2}}^{\frac{d_i}{2}} p_i(\mathbf{s}_i + r \mathbf{n}_i) dr. \quad (7)$$

Moreover, the reduced source term  $\hat{f}$  and the inverse of the scaled permeabilities  $\eta_\gamma$  and  $\hat{\eta}$  are defined as

$$\hat{f}_i(\mathbf{s}_i) := \int_{-\frac{d_i}{2}}^{\frac{d_i}{2}} f_i(\mathbf{s}_i + r \mathbf{n}_i) dr, \quad \eta_{\gamma_i} := \frac{d_i}{K_{i,\mathbf{n}}} \quad \text{and} \quad \hat{\eta}_i := \frac{1}{d_i K_{i,\boldsymbol{\tau}}}.$$

Using (7) and approximating  $\Gamma_i^{\mathbf{u}}$  with  $\partial\gamma_i^{\mathbf{u}}$  and  $\Gamma_i^p$  with  $\partial\gamma_i^p$ , so that  $\partial\gamma_i^{\mathbf{u}} \cap \partial\gamma_i^p = \emptyset$ , we obtain the corresponding reduced boundary data from the last two expressions of (5),

$$\hat{b}_{ij} := \int_{\partial\Omega_{ij} \cap \partial D} b_{ij}(\boldsymbol{\sigma}) d\boldsymbol{\sigma} \quad \text{and} \quad \hat{g}_{ij} := \frac{1}{|\partial\Omega_{ij} \cap \partial D|} \int_{\partial\Omega_{ij} \cap \partial D} g_{ij}(\boldsymbol{\sigma}) d\boldsymbol{\sigma}.$$

Indeed, by the definition in (7) we have that  $\hat{\mathbf{u}}_i \cdot \mathbf{n}_i = 0$  on  $\gamma_i$ , *i.e.*  $\hat{\mathbf{u}}_i$  is aligned to the tangential plane.

The reduced model on each  $\Omega_{ij}$  is obtained by integrating 3 along the fracture thickness and can then be written as

$$\begin{cases} \nabla_{\boldsymbol{\tau}_i} \cdot \hat{\mathbf{u}}_i = \hat{f}_i \\ \hat{\eta}_i \hat{\mathbf{u}}_i + \nabla_{\boldsymbol{\tau}_i} \hat{p}_i = \mathbf{0} \end{cases} \quad \text{in } \gamma_i \setminus \mathbf{i}_p, \quad \begin{cases} \hat{\mathbf{u}}_i \cdot \mathbf{n}_D = \hat{b}_i \\ \hat{p}_i = \hat{g}_i \end{cases} \quad \text{on } \partial\gamma_i^{\mathbf{u}} \quad \text{for } i = 1, 2.$$

We derive now a reduced model for the flow in the intersecting region  $I$  in order to find proper coupling conditions. To this aim, we assume that  $I$  can be modelled as a quadrilateral with parallel sides, *i.e.* the thicknesses  $d_i$  can be considered constant in  $I$ . Furthermore, we have assumed that the permeability tensor  $\mathbf{K}_I$  can be taken constant in  $I$ . Let us indicate with  $\boldsymbol{\tau}_i$  the tangential unit vector to  $\gamma_i$ , and with  $\boldsymbol{\tau}_{i,\mathbf{i}_p}$  its value at  $\mathbf{i}_p$ , and define  $d_i^* := d_i \sin \theta^{-1}$ , with  $\sin \theta = \sqrt{1 - (\boldsymbol{\tau}_{1,\mathbf{i}_p} \cdot \boldsymbol{\tau}_{2,\mathbf{i}_p})^2}$ . Then  $|I| = d_1^* d_2^* |\sin \theta|$ . Note that  $\theta$  is the angle between the two fractures at the intersection as shown in Figure 2. We can write the intersecting region as

$$I = \left\{ \mathbf{x} \in \Omega : \mathbf{x} = \mathbf{i}_p + x_1 \boldsymbol{\tau}_{1,\mathbf{i}_p} + x_2 \boldsymbol{\tau}_{2,\mathbf{i}_p}, x_i \in \left( -\frac{d_j^*}{2}, \frac{d_j^*}{2} \right) \text{ for } i \neq j = 1, 2 \right\},$$

see Figure 2 for an example. The reduction process approximates  $I$  with  $\mathbf{i}_p$  and assumes that the fluxes  $\hat{\mathbf{u}}_i$  and the pressures  $\hat{p}_i$  can be discontinuous at



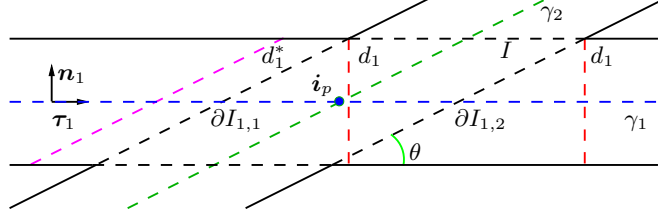


Figure 2: Example of an intersection.

$\mathbf{i}_p$ . Thus, we denote with  $\hat{p}_I \in \mathbb{R}$  the reduced value of the pressure at the intersection, defined as

$$\hat{p}_I := \frac{1}{|I|} \int_I p_I(\mathbf{x}) d\mathbf{x}. \quad (8)$$

The intersection point divides each line  $\gamma_i$  into two parts,  $\gamma_{i1}$  and  $\gamma_{i2}$  respectively, where the indexes 1 and 2 refer to the orientation induced by the tangent vectors. The double subscript  $ij$ , with  $i, j = 1, 2$ , will then be used to indicate quantities on  $\gamma_{ij}$ . Furthermore, since  $\hat{\mathbf{u}}_i$  is by definition aligned along  $\gamma_i$  we may write  $\hat{\mathbf{u}}_i = u_i \boldsymbol{\tau}_i$ .

We can then define the jump and mean operator across  $\mathbf{i}_p$  as

$$\llbracket a_i \rrbracket_{\mathbf{i}_p} := a_{i1} - a_{i2} \quad \text{and} \quad \{ \{ a_i \} \}_{\mathbf{i}_p} := \frac{a_{i1} + a_{i2}}{2}, \quad \text{for } i = 1, 2.$$

Thanks to (4), it is reasonable to make the following assumptions,

$$\int_{\partial I_{ij}} \mathbf{u}_I \approx \hat{\mathbf{u}}_{ij}(\mathbf{i}_p) \quad \text{and} \quad \frac{1}{d_i^*} \int_{\partial I_{ij}} p_I \approx \hat{p}_{ij}(\mathbf{i}_p), \quad \text{for } i, j = 1, 2.$$

Mass conservation implies that

$$\sum_{k=1}^2 \llbracket \hat{\mathbf{u}}_k \cdot \boldsymbol{\tau}_k \rrbracket_{\mathbf{i}_p} = \hat{f}_I \quad \text{with} \quad \hat{f}_I := \frac{1}{|I|} \int_I f_I(\mathbf{x}) d\mathbf{x}.$$

We integrate the first of (3) on  $I$ , approximating the integral involving the velocity  $\mathbf{u}_I$  by the trapezoidal rule on each fracture, to find

$$\int_I \mathbf{K}_I^{-1} \mathbf{u}_I \approx \mathbf{K}_I^{-1} \frac{|I|}{2} \sum_{k=1}^2 \frac{1}{d_k^*} (\hat{\mathbf{u}}_{k1} + \hat{\mathbf{u}}_{k2}) = \mathbf{K}_I^{-1} |I| \sum_{k=1}^2 \frac{1}{d_k^*} \{ \{ \hat{\mathbf{u}}_k \} \}_{\mathbf{i}_p}.$$

Furthermore the integral of the gradient of the pressure  $p_I$  in the intersection can be written as

$$\begin{aligned} \int_I \nabla p_I &= \sum_{i,j=1}^2 \mathbf{n}_{ij} \int_{\partial I_{ij}} p_I \approx (\hat{p}_{12} - \hat{p}_{11}) \mathbf{n}_2 d_1^* + (\hat{p}_{22} - \hat{p}_{21}) \mathbf{n}_1 d_2^* = \\ &= -\llbracket \hat{p}_1 \rrbracket_{\mathbf{i}_p} \mathbf{n}_2 d_1^* - \llbracket \hat{p}_2 \rrbracket_{\mathbf{i}_p} \mathbf{n}_1 d_2^*. \end{aligned}$$

Then, we obtain

$$\mathbf{K}_I^{-1} |I| \sum_{k=1}^2 \frac{1}{d_k^*} \{\{\hat{\mathbf{u}}_k\}\}_{\mathbf{i}_p} = \llbracket \hat{p}_1 \rrbracket_{\mathbf{i}_p} \mathbf{n}_2 d_1^* + \llbracket \hat{p}_2 \rrbracket_{\mathbf{i}_p} \mathbf{n}_1 d_2^*.$$

Multiplying the above relation by  $\boldsymbol{\tau}_1$ , or similarly by  $\boldsymbol{\tau}_2$ , using the identity  $d_1 = d_1^* \mathbf{n}_2 \cdot \boldsymbol{\tau}_1$  and the fact the  $\hat{\mathbf{u}}_i = (\hat{\mathbf{u}}_i \cdot \boldsymbol{\tau}_i) \boldsymbol{\tau}_i$  we obtain, for  $i = 1$  and  $2$ ,

$$\frac{|I|}{d_i} \sum_{k=1}^2 \frac{\eta_{ik}^I}{d_k^*} \{\{\hat{\mathbf{u}}_k \cdot \boldsymbol{\tau}_k\}\}_{\mathbf{i}_p} = \llbracket \hat{p}_i \rrbracket_{\mathbf{i}_p} \quad \text{in } \mathbf{i}_p, \quad (9)$$

where

$$\eta_{ij}^I := \boldsymbol{\tau}_{i, \mathbf{i}_p}^\top \cdot \mathbf{K}_I^{-1} \boldsymbol{\tau}_{j, \mathbf{i}_p}. \quad (10)$$

If  $\gamma_1$  and  $\gamma_2$  are orthogonal and the permeability tensor  $\mathbf{K}_I$  is such that

$$\mathbf{K}_I^{-1} = \eta_{\gamma_1} \boldsymbol{\tau}_{1, \mathbf{i}_p} \otimes \boldsymbol{\tau}_{1, \mathbf{i}_p} + \eta_{\gamma_2} \boldsymbol{\tau}_{2, \mathbf{i}_p} \otimes \boldsymbol{\tau}_{2, \mathbf{i}_p} \quad (11)$$

the coupling conditions (9) can be simplified yielding

$$\eta_{\gamma_i} \frac{d_j}{d_i} \{\{\hat{\mathbf{u}}_i \cdot \boldsymbol{\tau}_i\}\}_{\mathbf{i}_p} = \llbracket \hat{p}_i \rrbracket_{\mathbf{i}_p} \quad \text{in } \mathbf{i}_p, \text{ for } i, j = 1, 2, \quad j \neq i.$$

To close the system we derive now a model for the pressure at the intersection. For each fracture in the first half of the transversal section we approximate the value of the pressure in  $\mathbf{i}_p$  by the following truncated Taylor expansion

$$p_j(\mathbf{i}_p) = p_I(\mathbf{x}_1) + \frac{d_j^*}{2} \nabla p_I(\boldsymbol{\theta}_1) \cdot \boldsymbol{\tau}_i \quad \text{with } i \neq j, \quad (12)$$

where  $\boldsymbol{\theta}_1 = \mathbf{i}_p - \boldsymbol{\tau}_i \xi_1 d_j^*/2$  with  $\xi_1 \in [0, 1]$ , see Figure 3. In the second transversal

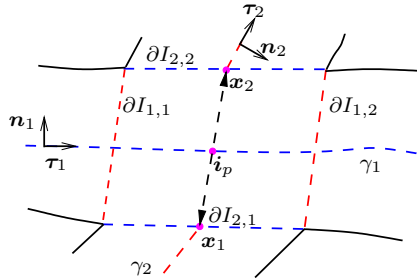


Figure 3: Example of a bi-dimensional intersection between two fractures.

section we approximate the value of the pressure in the intersection point  $\mathbf{i}_p$  by

$$p_j(\mathbf{i}_p) = p_I(\mathbf{x}_2) - \frac{d_j^*}{2} \nabla p_I(\boldsymbol{\theta}_2) \cdot \boldsymbol{\tau}_i \quad \text{with } i \neq j, \quad (13)$$

where  $\boldsymbol{\theta}_2 = \mathbf{i}_p + \boldsymbol{\tau}_i \xi_2 d_j^*/2$  with  $\xi_2 \in [0, 1]$ . Using (3) and (4) we find

$$p_j(\mathbf{i}_p) = p_{i,k} + (-1)^k \frac{d_j^*}{2} \boldsymbol{\tau}_i^\top \cdot \mathbf{K}_I^{-1} \mathbf{u}_I(\boldsymbol{\theta}_k) \quad \text{for } k = 1, 2. \quad (14)$$

The values of  $\mathbf{u}_I$  in both  $\boldsymbol{\theta}_1$  and  $\boldsymbol{\theta}_2$  are unknown, therefore we express them by the following convex combination for each fracture

$$\begin{aligned} \mathbf{u}_I(\boldsymbol{\theta}_1) &= \xi_1 \mathbf{u}_{1,1} + (1 - \xi_1) \mathbf{u}_{1,2} + \frac{1}{2} (\mathbf{u}_{2,1} + \mathbf{u}_{2,2}) \quad \text{for } \xi_1 \in [0, 1], \\ \mathbf{u}_I(\boldsymbol{\theta}_2) &= \xi_2 \mathbf{u}_{1,2} + (1 - \xi_2) \mathbf{u}_{1,1} + \frac{1}{2} (\mathbf{u}_{2,2} + \mathbf{u}_{2,1}) \quad \text{for } \xi_2 \in [0, 1]. \end{aligned}$$

Using the previous expression for  $\mathbf{u}_I$  and integrating in  $I$ , equation (14) becomes

$$\begin{aligned} \hat{p}_I &= \hat{p}_{i,1} - \boldsymbol{\tau}_i^\top \cdot \mathbf{K}_I^{-1} \left[ \frac{1}{2} \left( \frac{d_j}{d_i} \llbracket \hat{\mathbf{u}}_i \rrbracket_{\mathbf{i}_p} + \llbracket \hat{\mathbf{u}}_j \rrbracket_{\mathbf{i}_p} \right) + \hat{\xi}_{0,1} \frac{d_j}{d_i} \llbracket \hat{\mathbf{u}}_i \rrbracket_{\mathbf{i}_p} \right], \\ \hat{p}_I &= \hat{p}_{i,2} + \boldsymbol{\tau}_i^\top \cdot \mathbf{K}_I^{-1} \left[ \frac{1}{2} \left( \frac{d_j}{d_i} \llbracket \hat{\mathbf{u}}_i \rrbracket_{\mathbf{i}_p} + \llbracket \hat{\mathbf{u}}_j \rrbracket_{\mathbf{i}_p} \right) - \hat{\xi}_{0,2} \frac{d_j}{d_i} \llbracket \hat{\mathbf{u}}_i \rrbracket_{\mathbf{i}_p} \right], \end{aligned}$$

where  $\hat{\xi}_{0,k} := (2\xi_k - 1)/4$  for  $k = 1, 2$ . Finally using (9) and the fact that pressure  $\hat{p}_I$  is single valued, thus  $\hat{\xi}_{0,k} = \hat{\xi}_0$  for  $k = 1, 2$ , we obtain the last coupling condition of our reduced model

$$\hat{\xi}_0 \frac{d_j}{d_i} \eta_{ii}^I \llbracket \hat{\mathbf{u}}_i \cdot \boldsymbol{\tau}_i \rrbracket_{\mathbf{i}_p} = \llbracket \hat{p}_i \rrbracket_{\mathbf{i}_p} - \hat{p}_I \quad \text{in } \mathbf{i}_p, \quad (15)$$

To sum up, the complete reduced model that describes the evolution of  $\hat{\mathbf{u}}_i$ ,  $\hat{p}_i$  and  $\hat{p}_I$  consists of the following system of partial differential equations

$$\begin{cases} \nabla_{\boldsymbol{\tau}_i} \cdot \hat{\mathbf{u}}_i = \hat{f}_i, \\ \hat{\eta}_i \hat{\mathbf{u}}_i + \nabla_{\boldsymbol{\tau}_i} \hat{p}_i = \mathbf{0}, \end{cases} \quad \text{in } \gamma_i \setminus \mathbf{i}_p, \quad \begin{cases} \hat{\mathbf{u}}_i \cdot \mathbf{n}_D = \hat{b}_i & \text{on } \partial\gamma_i^u, \\ \hat{p}_i = \hat{g}_i & \text{on } \partial\gamma_i^p, \end{cases} \quad \text{for } i = 1, 2. \quad (16)$$

and the coupling conditions for the fracture-fracture system for  $i \neq j = 1, 2$ ,

$$\begin{cases} \sum_{k=1}^2 \llbracket \hat{\mathbf{u}}_k \cdot \boldsymbol{\tau}_k \rrbracket_{\mathbf{i}_p} = \hat{f}_I, \\ \frac{|I|}{d_i} \sum_{k=1}^2 \frac{\eta_{ik}^I}{d_k^*} \llbracket \hat{\mathbf{u}}_k \cdot \boldsymbol{\tau}_k \rrbracket_{\mathbf{i}_p} = \llbracket \hat{p}_i \rrbracket_{\mathbf{i}_p}, \\ \hat{\xi}_0 \frac{d_j}{d_i} \eta_{ii}^I \llbracket \hat{\mathbf{u}}_i \cdot \boldsymbol{\tau}_i \rrbracket_{\mathbf{i}_p} = \llbracket \hat{p}_i \rrbracket_{\mathbf{i}_p} - \hat{p}_I. \end{cases} \quad \text{in } \mathbf{i}_p. \quad (17)$$

If the intersection region has a high permeability then  $\eta_{ij}^I \approx 0$  and conditions (17) reduce to those in [1, 3], *i.e.* continuity of pressure and mass conservation. However, our model is more general as it allows for different choices of  $\mathbf{K}_I$ , and it is useful in practical situations where fractures have rather different permeabilities and may even act as barrier to the flow. This fact will be illustrated in the section dedicated to numerical experimentation.

## 4 Weak formulation and functional setting

We describe here the functional setting for homogeneous essential boundary conditions, *i.e.* all possible  $\hat{b}_i$  are set to zero, since the non-homogeneous case may be recovered by standard lifting techniques. For a given regular curve  $\gamma : (0, L) \rightarrow \mathbb{R}^2$  with tangent  $\boldsymbol{\tau}$  defined almost everywhere on  $\gamma$  we define the vector space

$$\mathbf{H}_{\text{div}}(\gamma) := \left\{ \mathbf{w} \in [L^2(\gamma)]^2 : \nabla_{\boldsymbol{\tau}} \cdot \mathbf{w} \in L^2(\gamma), \mathbf{w} \cdot \mathbf{n} = 0 \text{ and } \mathbf{w} \cdot \mathbf{n}_D = 0 \right\},$$

with norm

$$\|\mathbf{w}\|_{\mathbf{H}_{\text{div}}(\gamma)}^2 := \|\mathbf{w}\|_{L^2(\gamma)}^2 + \|\nabla_{\boldsymbol{\tau}} \cdot \mathbf{w}\|_{L^2(\gamma)}^2$$

Furthermore we assume here that elements of  $\mathbf{w} \in \mathbf{H}_{\text{div}}(\gamma)$  are aligned with  $\gamma$ , *i.e.* for a  $\mathbf{w} \in \mathbf{H}_{\text{div}}(\gamma)$  we have  $\mathbf{w} = w\boldsymbol{\tau}$ , with  $w \in H^1(\gamma)$ . We set  $\mathbf{W}_{ij} := \mathbf{H}_{\text{div}}(\gamma_{ij})$  and  $\mathbf{W}_i := \mathbf{W}_{i1} \times \mathbf{W}_{i2}$  with norm

$$\|\mathbf{w}_i\|_{\mathbf{W}_i}^2 := \|\mathbf{w}_{i1}\|_{\mathbf{W}_{i1}}^2 + \|\mathbf{w}_{i2}\|_{\mathbf{W}_{i2}}^2 + \|\mathbf{w}_i \cdot \boldsymbol{\tau}_i\|_{i_p}^2 \quad \text{where } \mathbf{w}_i = (\mathbf{w}_{i1}, \mathbf{w}_{i2}) \in \mathbf{W}_i.$$

Let  $Q_{ij} := L^2(\gamma_{ij})$  and  $Q_i := Q_{i1} \times Q_{i2}$ ,  $Q_i$  may be identified with  $L^2(\gamma_i)$ . We set  $\mathbf{W} := \mathbf{W}_1 \times \mathbf{W}_2$  with norm

$$\|\mathbf{w}\|_{\mathbf{W}}^2 := \|\mathbf{w}_1\|_{\mathbf{W}_1}^2 + \|\mathbf{w}_2\|_{\mathbf{W}_2}^2, \quad \text{where } \mathbf{w} = (\mathbf{w}_1, \mathbf{w}_2) \in \mathbf{W},$$

and  $Q := Q_1 \times Q_2 \times \mathbb{R}$  with norm

$$\|q\|_Q^2 := \|q_1\|_{Q_1}^2 + \|q_2\|_{Q_2}^2 + q_3^2, \quad \text{where } q = (q_1, q_2, q_3) \in Q.$$

All those spaces are in fact Hilbert spaces equipped with scalar products associated with the chosen norms.

To obtain the weak formulation of (16) we take a test function  $q_i \in Q_i$  and integrate on each branch  $\gamma_{i,j}$  the first equation in (16) to obtain, summing over  $j$

$$(\nabla_{\boldsymbol{\tau}_i} \cdot \hat{\mathbf{u}}_i, q_i)_{\gamma_i} = \left( \hat{f}_i, q_i \right)_{\gamma_i} \quad \forall q_i \in Q_i, \quad i = 1, 2.$$

Taking then a test function  $\mathbf{w}_i \in \mathbf{W}_i$  and integrating on each  $\gamma_{i,j}$  the second equation in (16) we obtain

$$\begin{aligned} (\hat{\eta}_i \hat{\mathbf{u}}_i, \mathbf{w}_i)_{\gamma_i} - (\hat{p}_{i,j}, \nabla_{\boldsymbol{\tau}_i} \cdot \mathbf{w}_i)_{\gamma_i} + \|\hat{p}_i \mathbf{w}_i \cdot \boldsymbol{\tau}_i\|_{i_p} + \sum_{ij: \partial\gamma_{ij}^p \neq \emptyset} \hat{g}_i(\mathbf{w}_i \cdot \mathbf{n}_D)|_{\partial\gamma_{ij}^p} = 0 \\ \forall \mathbf{w}_i \in \mathbf{W}_i, \quad i = 1, 2. \end{aligned}$$

Note that we have integrated by parts the pressure term and used the natural boundary conditions. Thanks to the identity  $\llbracket ab \rrbracket = \llbracket a \rrbracket \{ \! \! \{ b \} \! \! \} + \{ \! \! \{ a \} \! \! \} \llbracket b \rrbracket$  we can

include the coupling conditions (17) substituting the expression of the pressure jump and average in

$$\llbracket \hat{p}_i \mathbf{w}_i \cdot \boldsymbol{\tau}_i \rrbracket_{i_p} = \llbracket \hat{p}_i \rrbracket_{i_p} \{ \mathbf{w}_i \cdot \boldsymbol{\tau}_i \}_{i_p} + \{ \hat{p}_i \}_{i_p} \llbracket \mathbf{w}_i \cdot \boldsymbol{\tau}_i \rrbracket_{i_p}.$$

Introducing  $\hat{\mathbf{u}} := (\hat{\mathbf{u}}_1, \hat{\mathbf{u}}_2) \in \mathbf{W}$  and  $\hat{p} := (\hat{p}_1, \hat{p}_2, \hat{p}_I) \in Q$  and summing over  $i$  the weak formulation of the coupled problem (16) and (17) can be now written as: find  $(\hat{\mathbf{u}}, \hat{p}) \in \mathbf{W} \times Q$  such that

$$\begin{cases} \mathcal{A}(\hat{\mathbf{u}}, \mathbf{w}) + \mathcal{B}(\hat{p}, \mathbf{w}) = \mathcal{F}(\mathbf{w}) & \forall \mathbf{w} \in \mathbf{W} \\ \mathcal{B}(q, \hat{\mathbf{u}}) = \mathcal{Q}(q) & \forall q \in Q. \end{cases} \quad (18)$$

The functionals and bilinear forms in (18) are defined as

$$\mathcal{A}(\mathbf{u}, \mathbf{w}) := \sum_{i=1}^2 a_i(\mathbf{u}_i, \mathbf{w}_i) + \sum_{\substack{i,j=1 \\ i \neq j}}^2 \eta_{ij}^I \{ \mathbf{u}_j \cdot \boldsymbol{\tau}_j \}_{i_p} \{ \mathbf{w}_j \cdot \boldsymbol{\tau}_j \}_{i_p}, \quad (19a)$$

$$\mathcal{B}(q, \mathbf{w}) := \sum_{i=1}^2 -(q_i, \nabla_{\boldsymbol{\tau}_i} \cdot \mathbf{w}_i)_{L^2(\gamma_i)} + q_3 \llbracket \mathbf{w}_i \cdot \boldsymbol{\tau}_i \rrbracket_{i_p}, \quad (19b)$$

$$\mathcal{F}(\mathbf{w}) := \sum_{ij: \partial \gamma_{ij}^p \neq \emptyset} -\hat{g}_i(\mathbf{w}_i \cdot \mathbf{n}_D) |_{\partial \gamma_{ij}^p} \quad (19c)$$

$$\mathcal{Q}(q) := \sum_{i=1}^2 -(\hat{f}_i, q_i)_{L^2(\gamma_i)} + \hat{f}_I q_3. \quad (19d)$$

The bilinear forms  $a_i$  in  $\mathcal{A}$  are given, for  $i, j = 1, 2$  and  $i \neq j$ , by

$$a_i(\mathbf{u}, \mathbf{w}) := (\hat{\eta}_i \mathbf{u}, \mathbf{w})_{L^2(\gamma_i)} + \eta_{ii}^I \frac{d_j}{d_i} (\hat{\xi}_0 \llbracket \mathbf{u} \cdot \boldsymbol{\tau}_i \rrbracket_{i_p} \llbracket \mathbf{w} \cdot \boldsymbol{\tau}_i \rrbracket_{i_p} + \{ \mathbf{u} \cdot \boldsymbol{\tau}_i \}_{i_p} \{ \mathbf{w} \cdot \boldsymbol{\tau}_i \}_{i_p}). \quad (20)$$

We have the following

**Lemma 4.1 (Boundedness of  $\mathcal{A}$ )** *There exist a constant  $C \in \mathbb{R}^+$  such that*

$$|\mathcal{A}(\mathbf{u}, \mathbf{w})| \leq C \|\mathbf{u}\|_{\mathbf{W}} \|\mathbf{w}\|_{\mathbf{W}} \quad \forall \mathbf{u}, \mathbf{w} \in \mathbf{W}.$$

**Proof.**  $\mathcal{A}$  is clearly a bilinear form on  $\mathbf{W}$ . Since each  $\mathbf{u}_{ij}$  and  $\mathbf{w}_{ij}$  are aligned along  $\gamma_{ij}$ , that is  $\mathbf{u}_{ij} = u_{ij} \boldsymbol{\tau}_i$ , the request that  $\mathbf{u}_{ij} \in \mathbf{H}_{\text{div}}(\gamma_{ij})$  implies that  $u_{ij} \in H^1(\gamma_{ij})$ . Then the boundedness of  $\mathcal{A}$  can be obtained from the application Cauchy-Schwarz inequality together with Sobolev embeddings and trace inequalities, by which we can finally state that  $\exists C \in \mathbb{R}^+$  such that

$$|\mathcal{A}(\mathbf{u}, \mathbf{w})| \leq C \|\mathbf{u}\|_{\mathbf{W}} \|\mathbf{w}\|_{\mathbf{W}} \quad \text{where} \quad C = C \left( \|\hat{\eta}\|_{L^\infty(\gamma_1 \cup \gamma_2)}, \lambda_{max}, \bar{d}, c_\gamma \right)$$

with  $\bar{d} := \max_{i \neq j=1,2} d_i/d_j$  and  $c_\gamma$  depends on the trace inequality constants for each  $\gamma_{ij}$ .  $\square$

**Lemma 4.2 (Coercivity of  $\mathcal{A}$ )** *There exist a constant  $\alpha \in \mathbb{R}^+$  such that*

$$\mathcal{A}(\mathbf{u}, \mathbf{u}) \geq \alpha \|\mathbf{u}\|_{\mathbf{W}}^2 \quad \forall \mathbf{u} \in \mathbf{W}_0$$

where  $\mathbf{W}_0 := \{\mathbf{w} \in \mathbf{W} : \mathcal{B}(q, \mathbf{w}) = 0, \forall q \in Q\}$ .

**Proof.** By definition of  $\mathcal{B}$  we have that a  $\mathbf{w} \in \mathbf{W}_0$  is characterised by  $\nabla_{\boldsymbol{\tau}_i} \cdot \mathbf{w}_{ij} = 0$  almost everywhere on  $\gamma_{ij}$  and  $\llbracket \mathbf{w}_i \cdot \boldsymbol{\tau}_i \rrbracket_{i_p} = 0$ , for  $i, j = 1, 2$ . Therefore, for a  $\mathbf{w} \in \mathbf{W}_0$  we have  $\|\mathbf{w}\|_{\mathbf{W}}^2 = \sum_{i=1}^2 \|\mathbf{w}_i\|_{L^2(\gamma_i)}^2$ . Moreover, if  $\mathbf{w} \in \mathbf{W}_0$  we have

$$\mathcal{A}(\mathbf{w}, \mathbf{w}) = \sum_{i=1}^2 \left\| \eta_i^{1/2} \mathbf{w}_i \right\|_{L^2(\gamma_i)}^2 + \sum_{\substack{i,j=1 \\ i \neq j}}^2 \left( \eta_{ii}^I \frac{d_j}{d_i} \left\{ \mathbf{w}_i \cdot \boldsymbol{\tau}_i \right\}_{i_p}^2 + \eta_{ij}^I \left\{ \mathbf{w}_i \cdot \boldsymbol{\tau}_i \right\}_{i_p} \left\{ \mathbf{w}_j \cdot \boldsymbol{\tau}_j \right\}_{i_p} \right).$$

Let us introduce the vectors  $\mathbf{a}_i = \sqrt{d_j/d_i} \left\{ \mathbf{w}_i \cdot \boldsymbol{\tau}_i \right\}_{i_p} \boldsymbol{\tau}_i$ , for  $i, j = 1, 2$  and  $j \neq i$  and the scalar product  $(\mathbf{a}_1, \mathbf{a}_2)_K = \mathbf{a}_1^T \mathbf{K}_I^{-1} \mathbf{a}_2$ . We recall the definition of  $\eta_{ij}^I$  in (10) to note that the last sum in the previous equality may be written as

$$(\mathbf{a}_1, \mathbf{a}_1)_K + (\mathbf{a}_2, \mathbf{a}_2)_K + 2(\mathbf{a}_1, \mathbf{a}_2)_K = (\mathbf{a}_1 + \mathbf{a}_2, \mathbf{a}_1 + \mathbf{a}_2)_K \geq 0.$$

Therefore, the wanted inequality is proved with  $\alpha = \inf_{x \in \gamma_1 \cup \gamma_2} \hat{\eta}(x)$ .  $\square$

We indicate with  $M$  the set of indices  $ij$  corresponding to portions of fracture where we impose pressure boundary conditions, that is

$$M := \left\{ (i, j) : i, j = 1, 2 \text{ and } \partial\gamma_{ij} \cap \partial\gamma_{ij}^p \neq \emptyset \right\} \quad \text{and} \quad n_d := \#M.$$

**Theorem 4.1 (Inf-sup condition)** *If  $n_d > 0$ , then for all  $p \in Q$  there exist a  $\mathbf{w} \in \mathbf{W}$  with  $\mathbf{w} \neq \mathbf{0}$  such that*

$$\mathcal{B}(p, \mathbf{w}) \geq \beta \|p\|_Q \|\mathbf{w}\|_{\mathbf{W}},$$

for  $\beta \in \mathbb{R}^+$  independent on  $p$  and  $\mathbf{w}$ .

**Proof.** Given  $p = (\hat{p}_1, \hat{p}_2, \hat{p}_I) \in Q$  we construct the following auxiliary problems. For  $(i, j) \in M$  we look for function  $\phi_{ij} \in H^2(\gamma_{ij})$  such that

$$\begin{cases} -\nabla_{\boldsymbol{\tau}_i} \cdot (\nabla_{\boldsymbol{\tau}_i} \phi_{ij}) = \hat{p}_{ij} & \text{in } \gamma_{ij} \\ \frac{\partial \phi_{ij}}{\partial \boldsymbol{\tau}_i} = \frac{\hat{p}_I}{n_d} (-1)^{j+1} |\gamma| & \text{on } \mathbf{i}_p \\ \phi_{ij} = 0 & \text{on } \partial\gamma_{ij} \cap \partial\gamma_{ij}^p \end{cases} \quad (21)$$

with  $|\gamma| = \sum_i |\gamma_i|$ . While, for all other values of the indices  $i$  and  $j$  we look for the  $\phi_{ij}$  solution of

$$\begin{cases} -\nabla_{\boldsymbol{\tau}_i} \cdot (\nabla_{\boldsymbol{\tau}_i} \phi_{ij}) = \hat{p}_{ij} & \text{in } \gamma_{ij} \\ \frac{\partial \phi_{ij}}{\partial \boldsymbol{\tau}_i} = 0 & \text{on } \partial\gamma_{ij} \cap \partial\gamma_{ij}^u \\ \phi_{ij} = 0 & \text{on } \mathbf{i}_p \end{cases} \quad (22)$$

Both problems are well posed and enjoy elliptic regularity.

We consider  $\mathbf{w}_{ij} = \nabla_{\tau_i} \phi_{ij}$ . We have, by construction, that the solution of (21) provides at the intersection point  $\mathbf{i}_p$

$$\mathbf{w}_{ij} \cdot \boldsymbol{\tau}_i = \frac{\hat{p}_I}{n_d} (-1)^{j+1} |\gamma|. \quad (23)$$

For the solution of (22) by simple computations we derive that at  $\mathbf{i}_p$

$$\mathbf{w}_{ij} \cdot \boldsymbol{\tau}_i = - \int_{\gamma_{ij}} (-1)^{j+1} \hat{p}_{ij} d\gamma. \quad (24)$$

Furthermore,

$$\mathcal{B}(p, \mathbf{w}) = \sum_{i,j=1}^2 \|\hat{p}_{ij}\|_{L^2(\gamma_{ij})}^2 + |\gamma| \hat{p}_I^2 + \sum_{(i,j) \in M} \int_{\gamma_{ij}} \hat{p}_{ij} \hat{p}_I,$$

Thanks to Young's inequality applied to the third term, we have that

$$\mathcal{B}(p, \mathbf{w}) \geq \frac{1}{2} \left( \sum_{i,j=1}^2 \|\hat{p}_{ij}\|_{L^2(\gamma_{ij})}^2 + |\gamma| \hat{p}_I^2 \right) \geq c \|p\|_Q^2,$$

with  $c = \frac{1}{2} \min\{1, |\gamma|\}$ . Exploiting standard stability results for the solution of (21) and (22), we infer that

$$\sum_{i=1}^2 \|\mathbf{w}_{ij}\|_{L^2(\gamma_{ij})}^2 = \sum_{i=1}^2 \|\nabla_{\tau_i} \phi_{ij}\|_{L^2(\gamma_{ij})}^2 \leq C \left( \hat{p}_I^2 + \sum_{i=1}^2 \|\hat{p}_{ij}\|_{L^2(\gamma_{ij})}^2 \right),$$

moreover we have

$$\begin{aligned} \sum_{i=1}^2 \|\nabla_{\tau_i} \cdot \mathbf{w}_{ij}\|_{L^2(\gamma_{ij})}^2 &= \sum_{i=1}^2 \|\nabla_{\tau_i} \cdot (\nabla_{\tau_i} \phi_{ij})\|_{L^2(\gamma_{ij})}^2 = \\ &= \sum_{i=1}^2 \|\phi_{ij}\|_{H^2(\gamma_{ij})}^2 \leq C \left( \hat{p}_I^2 + \sum_{i=1}^2 \|\hat{p}_{ij}\|_{L^2(\gamma_{ij})}^2 \right) \end{aligned}$$

Thus,  $\sum_{ij} \|\mathbf{w}_{ij}\|_{\mathbf{W}_{ij}}^2 \lesssim \|p\|_Q^2$ . Furthermore,  $\|\mathbf{w}_i\|_{\mathbf{i}_p}^2 \lesssim \|p_i\|_{Q_i}^2 + \hat{p}_I^2$  because of (24) and (23). In conclusion there exist a constant  $C \in \mathbb{R}^+$  such that  $\|\mathbf{w}\|_{\mathbf{W}} \leq C \|p\|_Q$ . This result allows us to complete the proof.  $\square$

**Remark 2** *The condition  $n_d \geq 1$  in the previous proof is needed, otherwise we are not able to control the pressure  $\hat{p}_I$ . However, if all boundary conditions are imposed on the velocity we are still able to find a solution provided that the boundary velocity satisfy a global mass conservation. In this case, however,  $\hat{p}_{ij} \in L^2(\gamma) \setminus \mathbb{R}$  and  $\hat{p}_I$  may take any arbitrary value.*

**Lemma 4.3 (Boundedness of  $\mathcal{F}$  and  $\mathcal{Q}$ )** *There exists  $C_1, C_2 \in \mathbb{R}^+$  such that*

$$|\mathcal{F}(\mathbf{w})| \leq C_1 \|\mathbf{w}\|_{\mathbf{W}} \quad \text{and} \quad |\mathcal{Q}(q)| \leq C_2 \|q\|_Q \quad \forall (\mathbf{w}, q) \in \mathbf{W} \times Q.$$

**Proof.** Let  $(i, j) \in M$ , then  $(\mathbf{w}_{ij} \cdot \mathbf{n}_D)|_{\partial\gamma_{ij}^p}$  satisfies

$$|\mathbf{w}_{ij} \cdot \mathbf{n}_D| \leq |w_{ij}| |\boldsymbol{\tau}_i \cdot \mathbf{n}_D| \leq |w_{ij}| \leq C_{\gamma_{ij}} \|w_{ij}\|_{H^1(\gamma_{ij})} \leq C_{\gamma_{ij}} \|\mathbf{w}_{ij}\|_{\mathbf{w}_{ij}} \leq C_{\gamma_{ij}} \|\mathbf{w}\|_{\mathbf{w}}.$$

We have used the trace inequality for functions in  $H^1$ . By summing over all  $(i, j) \in M$  we have

$$|\mathcal{F}(\mathbf{w})| \leq \max_{ij: \partial\gamma_{ij}^p \neq \emptyset} (|\hat{g}_{ij}| C_{\gamma_{ij}}) \|\mathbf{w}\|_{\mathbf{w}}.$$

Furthermore

$$|\mathcal{Q}(q)| \leq \sum_{i=1}^2 \|\hat{f}_i\|_{L^2(\gamma_i)} \|q_i\|_{L^2(\gamma_i)} + |\hat{f}_I| |q_3| \leq \left( \sum_{i=1}^2 \|\hat{f}_i\|_{L^2(\gamma_i)} + |\hat{f}_I| \right) \|q\|_{\mathcal{Q}}.$$

□

Thanks to the previous results problem (18) is well posed, [6].

We state now a maximum principle for the continuous problem (18). It is well known that the original problem in  $\Omega_1 \cup \Omega_2$  expressed by (3) satisfies a maximum principle for the pressure. Namely, in the absence of the source terms  $f_i$  and  $f_I$  a smooth pressure solution is always within the maximal and minimal value taken at the boundary. We verify the conditions under which a similar property is enjoyed by the solution of the reduced model.

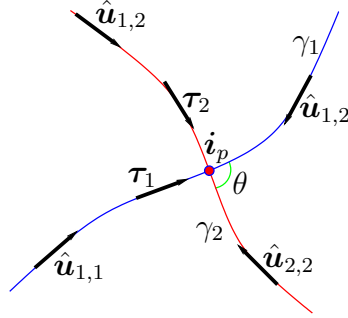


Figure 4: Example of an intersection with the convention of the directions for Theorem 4.2.

**Theorem 4.2 (Maximum principle)** *In the case  $\hat{f}_i = 0$  and  $\hat{f}_I = 0$ , if the permeability tensor  $\mathbf{K}_I$  is isotropic and if the parameter  $\hat{\xi}_0$  is such that*

$$\frac{\sin^2(\theta)}{4(d_{1,2}^2 + 1)} \leq \hat{\xi}_0 \leq \frac{d_{1,2}}{4(d_{1,2}^2 + 1)} \frac{\sin^2(\theta)}{\cos(\theta)},$$

where  $d_{1,2} = d_1/d_2$ , then a maximum principle is satisfied by problem (16) coupled with (17). In particular, given a smooth solution  $\hat{p}$  we have that all pressures  $\hat{p}_{ij}$  in  $\gamma_{ij}$ , as well as  $\hat{p}_I$  are within the values taken by the pressure at boundaries  $\partial\gamma_{ij} \cap \partial D$ .



**Proof.** Let  $\hat{\mathbf{u}}$  and  $\hat{p}$  be a solution of the reduced model (16) with  $\hat{f}_i = 0$  and  $\hat{f}_I = 0$ . Each  $p_{ij}$  enjoys the maximum principle on  $\gamma_{ij}$ . To prove that this is the case also for the global problem it is sufficient to prove that: (a) the reduced pressures in the fractures at the intersection point can be expressed as convex combinations of the pressures at the external boundaries; (b) the pressure  $\hat{p}_I$  is a convex combination of the pressures in the fractures at the intersection.

The tangent vectors  $\boldsymbol{\tau}_i$  are continuous at  $\mathbf{i}_p$ . Without loss of generality we choose a frame of reference such that  $\boldsymbol{\tau}_{1,2} = (1 + m^2)^{-1}[1, \mp m]^\top$ , with  $m = \tan \theta/2$  and  $0 < |m| < 1$ , where  $\theta$  is the angle between fractures as Figure 4 shows. Moreover, since the numbering of the fractures is arbitrary we suppose that  $d_{1,2} \leq 1$ . Since we have assumed that the permeability tensor at the intersection  $\mathbf{K}_I$  is isotropic we set  $\mathbf{K}_I = \eta_i \mathbf{I}$ .

Let us indicate with  $\bar{p}_{ij}$  the value of  $p_{ij}$  at  $\mathbf{i}_p$  and with  $g_{ij}$  the value at the corresponding external boundary point of  $\gamma_{ij}$ . Then, by integrating (16), we get, referring to Figure 2,

$$\bar{p}_{ij} - g_{ij} = \hat{p}_i(L_{ij}) - \hat{p}_{ij}(0) = - \int_0^{L_{ij}} \hat{\eta}_i \hat{u}_{ij} ds = - \hat{u}_{ij} \int_0^{L_{ij}} \hat{\eta}_i ds, \quad (25)$$

where we have denoted with  $L_{ij}$  the length of the  $j$ -th branch of  $\gamma_i$ , and set  $\hat{u}_{ij} = \pm \hat{\mathbf{u}}_i \cdot \boldsymbol{\tau}_i$  with the convention that  $\hat{u}_{ij}$  is directed towards the intersection. Note that  $\hat{u}_{ij}$  is constant because of the continuity equation and the absence of source term.

We introduce the following vectors  $\mathbf{p} = [\bar{p}_{11}, \bar{p}_{12}, \bar{p}_{21}, \bar{p}_{22}]^\top$ ,  $\mathbf{g} = [g_{11}, g_{12}, g_{21}, g_{22}]^\top$  and  $\mathbf{u} = [\hat{u}_{11}, \hat{u}_{12}, \hat{u}_{21}, \hat{u}_{22}]^\top$  and matrix

$$\mathbf{D} = \text{diag} \{D_{11}, D_{12}, D_{21}, D_{22}\} \quad \text{with} \quad D_{ij} = - \int_0^{L_{ij}} \hat{\eta}_i ds.$$

Relation (25) may be rewritten as

$$\mathbf{u} = \mathbf{D}^{-1}(\mathbf{g} - \mathbf{p}). \quad (26)$$

Moreover, by manipulating the interface conditions (17) we are able to write

$$\mathbf{A}\mathbf{p} = \mathbf{u}. \quad (27)$$

Now we show that  $\mathbf{A}$  is such that  $\ker(\mathbf{A}) = \text{span}([1, 1, 1, 1]^\top)$ , and that  $-\mathbf{A}$  is a Z-matrix for some values of the parameter  $\hat{\xi}_0$ . The entries of the matrix can be written as  $A_{ij} = A_{N_{ij}} [4 \hat{\xi}_0 \eta_I m^2 d_2 (d_1^2 + d_2^2)]^{-1}$ , where  $A_{N_{ij}}$  read:

$$\begin{aligned} A_{N_{1,1}} &= A_{N_{2,2}} = -d_1 \left( \hat{\xi}_0 (d_1^2 + d_2^2) (1 + m^2)^2 + d_2^2 m^2 \right) \\ A_{N_{3,3}} &= A_{N_{4,4}} = -d_2^2 d_1^{-1} \left( \hat{\xi}_0 (d_1^2 + d_2^2) (1 + m^2)^2 + d_1^2 m^2 \right) \\ A_{N_{1,2}} &= A_{N_{2,1}} = d_1 \left( \hat{\xi}_0 (d_1^2 + d_2^2) (1 + m^2)^2 - d_2^2 m^2 \right) \\ A_{N_{1,3}} &= A_{N_{3,1}} = A_{N_{2,4}} = A_{N_{4,2}} = d_2 \left( \hat{\xi}_0 (d_1^2 + d_2^2) (1 - m^4) + d_1 d_2 m^2 \right) \\ A_{N_{1,4}} &= A_{N_{4,1}} = A_{N_{2,3}} = A_{N_{3,2}} = d_2 \left( -\hat{\xi}_0 (d_1^2 + d_2^2) (1 - m^4) + d_1 d_2 m^2 \right) \\ A_{N_{3,4}} &= A_{N_{4,3}} = d_2^2 d_1^{-1} \left( \hat{\xi}_0 (d_1^2 + d_2^2) (1 + m^2)^2 - d_1^2 m^2 \right) \end{aligned}$$

It can be verified directly that each row of the matrix sums to zero, which proves that the kernel of the matrix contains the constant vector.

The diagonal elements of  $\mathbf{A}$  are negative for any  $\hat{\xi}_0 \geq 0$  therefore  $-\mathbf{A}$  is a Z-matrix if the off-diagonal elements of  $\mathbf{A}$  are positive. It follows that the parameter  $\hat{\xi}_0$  must satisfy the following system of inequalities

$$\begin{aligned} \hat{\xi}_0 &\geq \frac{1}{d_{1,2}^2 + 1} \frac{m^2}{(1 + m^2)^2} & \hat{\xi}_0 &\geq \frac{d_{1,2}^2}{d_{1,2}^2 + 1} \frac{m^2}{(1 + m^2)^2} \\ (1 - m^2)\hat{\xi}_0 &\geq -\frac{d_{1,2}}{d_{1,2}^2 + 1} \frac{m^2}{(1 + m^2)} & (1 - m^2)\hat{\xi}_0 &\leq \frac{d_{1,2}}{d_{1,2}^2 + 1} \frac{m^2}{(1 + m^2)} \end{aligned}$$

Since  $|m| < 1$  the third inequality is satisfied for all  $\hat{\xi}_0$  and, since  $d_{1,2} \leq 1$ , the first constraint is at least as restrictive as the second. The system can thus be rewritten as

$$\frac{\sin^2(\theta)}{4(d_{1,2}^2 + 1)} \leq \hat{\xi}_0 \leq \frac{d_{1,2}}{4(d_{1,2}^2 + 1)} \frac{\sin^2(\theta)}{\cos(\theta)}.$$

We highlight that the bounds depends both on the angle  $\theta$  and on the ratio of the thicknesses, but not on the permeability. Combining (27) and (26) we can write

$$(\mathbf{I} + \mathbf{D}^{-1}\mathbf{A})\mathbf{p} = \mathbf{g}$$

Since  $\mathbf{D}$  is negative and  $\mathbf{A}$  has the aforementioned properties  $\mathbf{I} + \mathbf{D}^{-1}\mathbf{A}$  is an M-matrix whose rows sum to one, therefore the pressures  $\bar{p}_{ij}$  are convex combinations of the boundary values  $\mathbf{g}$ .

We need now to verify that  $\hat{p}_I$  is a convex combination of the  $\bar{p}_{ij}$ . Summing the two interface conditions (17) we get  $\hat{p}_I = \frac{1}{4} \sum_{i,j=1}^2 \bar{p}_{ij} - \xi_0 d_{1,2}^{-1} \eta_{ii}^I \sum_{i,j=1}^2 \hat{u}_{ij}$ , which becomes by using (27),  $\hat{p}_I = \mathbf{e}^T \left( \frac{1}{4} \mathbf{I} - \xi_0 d_{1,2}^{-1} \eta_{ii}^I \mathbf{A} \right) \mathbf{p}$ , where  $\mathbf{e}^T = [1, 1, 1, 1]$ . Because of the stated properties of  $\mathbf{A}$ , the vector  $\mathbf{e}^T (1/4 \mathbf{I} - \xi_0 d_{1,2}^{-1} \eta_{ii}^I \mathbf{A})$  has all positive entries which sum to one, then  $\hat{p}_I$  is a convex combination of the pressures  $\mathbf{p}$ , which completes the proof.  $\square$

## 5 Numerical discretization

We still consider two fractures with a single intersection, the extension to more general cases being straightforward. We discretize each curve  $\gamma_i$ ,  $i = 1, 2$  with a polygonal line  $\gamma_{h,i}$  with vertexes  $\mathbf{x}_{i,k} \in \gamma_i$ , for  $k = 1, \dots, N_{h,i}$ , and  $\mathbf{x}_k \neq \mathbf{i}_p$ . Clearly,  $\mathbf{x}_{i,1}$  and  $\mathbf{x}_{i,N_{h,i}}$  correspond the ends of the curve. For the sake of notation, we indicate with the same symbol  $\gamma_{h,i}$  the polygonal line and the mesh formed by the union of the line elements  $l_{i,k} = [\mathbf{x}_{i,k-1}, \mathbf{x}_k]$ . Moreover, we set  $h_{i,k} = |l_{i,k}|$  and  $h_i = \max_k h_{i,k}$ , while  $h = \max(h_1, h_2)$ .

Let  $l_{i,k}^c$  be the curved element on  $\gamma_i$  with the same end points of  $l_{i,k} \in \gamma_{h,i}$ . If the mesh is fine enough there exists a unique mapping  $\mathcal{F}_i : \gamma_i \rightarrow \gamma_{h,i}$  defined on each  $l_{i,k} \in \gamma_{h,i}$  by

$$\mathbf{x} = \mathbf{y} - D_i(\mathbf{y})\mathbf{n}_{h,i} \quad \text{for } \mathbf{x} \in l_{i,k} \quad \text{and} \quad \mathbf{y} \in l_{i,k}^c.$$

Here,  $\mathbf{n}_h$  is the normal vector to  $\gamma_{h,i}$ , which is piecewise constant in each  $l_{i,k}$ , and  $D_i(\mathbf{y}) := \text{dist}(\mathbf{y}, \gamma_{h,i})$ . The collection of the curved elements  $l_{i,k}^c$  will be denoted by  $\gamma_{h,i}^c$ , which geometrically coincides with  $\gamma_i$ . Because of the assumptions made on the regularity of  $\gamma_i$ , and in particular the boundedness on the curvature, we have that  $|D(\mathbf{y})| = \mathcal{O}(h^2)$  for all  $\mathbf{y} \in \gamma_i$ . If we indicate with  $\dot{D}_i$  the rate of variation of  $D_i(\mathbf{y})$  along  $\gamma_{h,i}$ , we may note that the arc length measures on  $\gamma_i$  and  $\gamma_{h,i}$  satisfy

$$d\gamma_i = (1 + \dot{D}_i^2)^{1/2} d\gamma_{h,i}.$$

We assume that the mesh is fine enough so that  $\dot{D}_i = \mathcal{O}(h)$  and, in particular, we have  $\dot{D}_i \in L^\infty(\gamma_{h,i})$ . By properly selecting the orientation of the curves we have the useful relations

$$\mathbf{n}_{h,i} \cdot \boldsymbol{\tau}_i = \dot{D}_i(1 + \dot{D}_i^2)^{-1/2}, \quad \boldsymbol{\tau}_i \cdot \boldsymbol{\tau}_{h,i} = (1 + \dot{D}_i^2)^{-1/2}, \quad (28)$$

where  $\boldsymbol{\tau}_{h,i}$  is the (piecewise constant) tangent vector of  $\gamma_{h,i}$ . Furthermore, we have that  $(1 + \dot{D}_i^2)^{-1/2} = 1 + \mathcal{O}(h)$ . Let now  $f : \gamma_{h,i} \rightarrow \mathbb{R}$ , we consider the transformations  $\mathcal{P}_i$  given by

$$f^c = \mathcal{P}_i f = f \circ \mathcal{F}_i. \quad (29)$$

Clearly,  $f^c : \gamma_i \rightarrow \mathbb{R}$ .

For a vector function  $\mathbf{v} : \gamma_{h,i} \rightarrow \mathbb{R}^2$  aligned with  $\gamma_{h,i}$ , *i.e.*  $\mathbf{v} = v\boldsymbol{\tau}_{h,i}$ , we consider instead the transformation  $\mathcal{P}_i$  given by

$$\mathbf{v}^c = \mathcal{P}_i \mathbf{v} = (v \circ \mathcal{F}_i) \cdot \boldsymbol{\tau}_{h,i} \boldsymbol{\tau}_i = (v \circ \mathcal{F}_i) \boldsymbol{\tau}_{h,i} \otimes \boldsymbol{\tau}_i.$$

**Lemma 5.1** *Transformation  $\mathcal{P}_i$  is an isomorphism between  $H^1(\gamma_{h,i})$  and  $H^1(\gamma_i)$ , while transformation  $\mathcal{P}_i$  is an isomorphism between  $\mathbf{H}_{\text{div}}(\gamma_{h,i})$  and  $\mathbf{H}_{\text{div}}(\gamma_i)$ . Furthermore,*

$$\int_{\gamma_i} \nabla_{\boldsymbol{\tau}_i} \cdot \mathbf{v}^c q^c d\gamma = \int_{\gamma_{h,i}} \nabla_{\boldsymbol{\tau}_{h,i}} \cdot \mathbf{v} q d\gamma \quad (30)$$

for all  $q \in L^2(\gamma_{h,i})$ ,  $\mathbf{v} \in \mathbf{H}_{\text{div}}(\gamma_{h,i})$  with  $q^c = \mathcal{P}_i q$  and  $\mathbf{v}^c = \mathcal{P}_i \mathbf{v}$ , respectively. Moreover, for each element  $l_{h,i}$  of  $\gamma_{h,i}$

$$|\nabla_{\boldsymbol{\tau}_{h,i}} \cdot \mathbf{v}|_{\mathbf{H}^1(l_{h,i})} = \|\nabla_{\boldsymbol{\tau}_{h,i}} \nabla_{\boldsymbol{\tau}_{h,i}} \cdot \mathbf{v}\|_{L^2(l_{h,i})} \lesssim |\nabla_{\boldsymbol{\tau}_i} \cdot \mathbf{v}^c|_{\mathbf{H}^1(l_{h,i}^c)} + h \|\nabla_{\boldsymbol{\tau}_i} \cdot \mathbf{v}^c\|_{L^2(l_{h,i}^c)} \quad (31)$$

**Proof.** By standard integration rules

$$\|f^c\|_{L^2(\gamma_i)}^2 = \int_{\gamma_i} (f^c)^2 d\gamma = \int_{\gamma_{h,i}} (1 + \dot{D}_i^2)^{1/2} f^2 d\gamma$$

Thus,

$$\|f\|_{L^2(\gamma_{h,i})}^2 \leq \|f^c\|_{L^2(\gamma_i)}^2 \leq C_h \|f\|_{L^2(\gamma_{h,i})}^2 \quad (32)$$

with  $C_h = 1 + \mathcal{O}(h) \geq 1$ . By the same technique we prove that

$$\|\mathbf{v}\|_{L^2(\gamma_{h,i})}^2 \leq \|\mathbf{v}^c\|_{L^2(\gamma_i)}^2 \leq C_h \|\mathbf{v}\|_{L^2(\gamma_{h,i})}^2. \quad (33)$$

We now note that if  $s$  and  $t$  denote the arch length coordinates along  $\gamma_i$  and  $\gamma_{h,i}$ , respectively, for a vector function  $\mathbf{v} = v\boldsymbol{\tau}_{h,i}$  aligned along  $\gamma_{h,i}$  we have the identities

$$\nabla_{\boldsymbol{\tau}_{h,i}} \cdot \mathbf{v} = \frac{dv}{dt} \quad \text{and} \quad \nabla_{\boldsymbol{\tau}_i} \cdot \mathbf{v}^c = \frac{dv^c}{ds}. \quad (34)$$

Thus,

$$\nabla_{\boldsymbol{\tau}_i} \cdot \mathbf{v}^c = \frac{dv \circ \mathcal{F}_i}{ds} = \frac{dv}{dt} \frac{dt}{ds} = (1 + \dot{D}_i^2)^{-1/2} \nabla_{\boldsymbol{\tau}_{h,i}} \cdot \mathbf{v}, \quad (35)$$

since  $ds/dt = (1 + \dot{D}_i^2)^{1/2}$ . Consequently,

$$c_h \|\nabla_{\boldsymbol{\tau}_{h,i}} \cdot \mathbf{v}\|_{L^2(\gamma_{h,i})} \leq \|\nabla_{\boldsymbol{\tau}_i} \cdot \mathbf{v}^c\|_{L^2(\gamma_i)} \leq \|\nabla_{\boldsymbol{\tau}_{h,i}} \cdot \mathbf{v}\|_{L^2(\gamma_{h,i})}$$

where  $c_h$  is a positive constant that behaves as  $c_h = 1 - \mathcal{O}(h)$ . Combining this last result with (32) we get

$$c_h \|\mathbf{v}\|_{\mathbf{H}_{\text{div}}(\gamma_{h,i})} \leq \|\mathbf{v}^c\|_{\mathbf{H}_{\text{div}}(\gamma_i)} \leq C_h \|\mathbf{v}\|_{\mathbf{H}_{\text{div}}(\gamma_{h,i})}. \quad (36)$$

Analogously,

$$\nabla_{\boldsymbol{\tau}_i} f^c = \frac{df^c}{ds} \boldsymbol{\tau}_i \quad \text{and} \quad \nabla_{\boldsymbol{\tau}_{h,i}} f = \frac{df}{dt} \boldsymbol{\tau}_{h,i}.$$

Thus,

$$\nabla_{\boldsymbol{\tau}_i} f^c = \frac{df \circ \mathcal{F}_i}{dt} \frac{dt}{ds} \boldsymbol{\tau}_i = (1 + \dot{D}_i^2)^{-1/2} \nabla_{\boldsymbol{\tau}_{h,i}} f \cdot \boldsymbol{\tau}_{h,i} \boldsymbol{\tau}_i.$$

Taking the  $L^2$  norm and applying the definition of the  $H^1(\gamma_{h,i})$  semi-norm we obtain

$$c_h |f|_{H^1(\gamma_{h,i})} \leq |f^c|_{H^1(\gamma_i)} \leq C_h |f|_{H^1(\gamma_{h,i})}. \quad (37)$$

As for (31) we use again the parametric representation to note that on each element  $l_{h,i}$

$$\begin{aligned} \nabla_{\boldsymbol{\tau}_i} \nabla_{\boldsymbol{\tau}_i} \cdot \mathbf{v}_{h,i}^c &= \frac{d}{ds} (\nabla_{\boldsymbol{\tau}_i} \cdot \mathbf{v}_{h,i}^c) \boldsymbol{\tau}_i = \frac{d}{dt} \left[ (1 + \dot{D}^2)^{-1/2} \nabla_{\boldsymbol{\tau}_{h,i}} \cdot \mathbf{v}_{h,i} \right] \boldsymbol{\tau}_i \\ &= (1 + \dot{D}^2)^{-1/2} \frac{d^2}{dt^2} v_{h,i} \boldsymbol{\tau}_i - \frac{\dot{D}\ddot{D}}{(1 + \dot{D}^2)^2} \frac{d}{dt} v_{h,i} \boldsymbol{\tau}_i = \\ &= (1 + \dot{D}^2)^{-1/2} \boldsymbol{\tau}_i \otimes \boldsymbol{\tau}_{h,i} \nabla_{\boldsymbol{\tau}_{h,i}} \nabla_{\boldsymbol{\tau}_{h,i}} \cdot \mathbf{v}_{h,i} - \frac{\dot{D}\ddot{D}}{(1 + \dot{D}^2)} \nabla_{\boldsymbol{\tau}_i} \cdot \mathbf{v}_{h,i}^c \boldsymbol{\tau}_i, \end{aligned}$$

where it is understood that quantities are computed on corresponding points on  $l_{h,i}$  and  $l_h$ , and we have used (34) and (35). By taking the  $L^2$  norm and using the fact that

$\dot{D} = \mathcal{O}(h)$  we obtain the wanted result. Finally, relation (30) is readily proved using (35) and applying the usual integration rules.  $\square$

We are now in the position of setting up our discrete spaces. We start by defining, for  $i = 1, 2$ ,

$$\mathbb{RT}_0(\gamma_{h,i}) = \{ \mathbf{w} \in \mathbf{H}_{\text{div}}(\gamma_{h,i}) : \mathbf{w} \in \mathbb{P}_1(l), \forall l \in \gamma_{h,i}, \mathbf{w} = w \boldsymbol{\tau}_{h,i}, w \in C^0(\gamma_{h,i}) \}$$

Note that despite the fact that  $\boldsymbol{\tau}_{h,i}$  is only piecewise continuous the tangential component of elements of  $\mathbb{RT}_0(\gamma_{h,i})$  is continuous. We also remind that, since we are treating problems on a one dimensional manifold, elements of  $\mathbf{H}_{\text{div}}(\gamma_{h,i})$  have tangential component in  $H^1$  and thus admit a continuous representative. The degrees of freedom on  $\mathbb{RT}_0(\gamma_{h,i})$  are indeed the values of  $w = \mathbf{w} \cdot \boldsymbol{\tau}_{h,i}$  at the mesh nodes. Correspondingly we have a set of basis function which we indicate as  $\{ \boldsymbol{\psi}_{i,k}, k = 1, \dots, N_{h,i} \}$ .

To account for the discontinuity at the intersection we consider the points  $\widehat{\mathbf{i}}_p = \mathcal{F}_i^{-1}(\mathbf{i}_p)$  projection of  $\mathbf{i}_p$  on  $\gamma_{h,i}$  and we enrich the space using the XFEM [12] methodology.

More precisely, let  $\mathcal{C}_{h,i} = [\mathbf{x}_{i,k-1}, \mathbf{x}_{i,k}]$  be the element crossed by the projected intersection point and  $\chi_{i,1}$  and  $\chi_{i,2}$  the characteristic functions of the sub-elements  $l_{i,1}^X = [\mathbf{x}_{i,k-1}, \widehat{\mathbf{i}}_p]$  and  $l_{i,2}^X = [\widehat{\mathbf{i}}_p, \mathbf{x}_{i,k}]$ , respectively. We consider the space

$$\mathbf{E}_u(\gamma_{h,i}) := \{ \mathbf{v}_{h,i} : \mathbf{v}_{h,i} = v_{i,1}^* \boldsymbol{\psi}_{i,k} \chi_{i,1} + v_{i,2}^* \boldsymbol{\psi}_{i,k-1} \chi_{i,2} \}.$$

The spaces  $\mathbb{RT}_0$  and  $\mathbf{E}_u$  have been defined on  $\gamma_{h,i}$ , we can then project them on the curve and account for essential boundary conditions by defining

$$\mathbf{W}_{h,i}^c := \mathcal{P}_i(\mathbb{RT}_0(\gamma_{h,i}) \oplus \mathbf{E}_p(\gamma_{h,i})) \cap \mathbf{W}_i. \quad (38)$$

Correspondingly,  $\mathbf{W}_{h,i} = \mathcal{P}_i^{-1}(\mathbf{W}_{h,i}^c)$ . By construction,  $\mathbf{W}_{h,i} \subset \mathbb{RT}_0(\gamma_{h,i}) \oplus E(\gamma_{h,i})$ .

**Remark 3** *The points  $\mathcal{F}_i^{-1}(\mathbf{i}_p)$  are in general different, unless the fractures  $\gamma_i$  are straight lines, and  $\| \mathcal{F}_1^{-1}(\mathbf{i}_p) - \mathcal{F}_2^{-1}(\mathbf{i}_p) \| = \mathcal{O}(h^2)$  as  $h \rightarrow 0$ . However, in most practical situations fractures are almost straight and for a sufficiently fine mesh the distance of the two projection is rather small. For this reason, and for the sake of notation, we have used a unique symbol,  $\widehat{\mathbf{i}}_p$  for both projected intersection points.*

For the pressure we proceed by setting

$$Q_{h,i} := \{ q \in L^2(\gamma_{h,i}) : q|_l = q_{il}, \forall l \in \gamma_{h,i} \setminus \mathcal{C}_{h,i}, q|_{\mathcal{C}_{h,i}} = q_{i1}^* \chi_{i,1} + q_{i2}^* \chi_{i,2} \},$$

which is the extended space of piecewise constant functions on  $\gamma_{h,i}$ , and we lift it to  $\gamma_i$ , by defining  $Q_{h,i}^c := \mathcal{P}_i(Q_{h,i})$ . The space  $Q_{h,i}^c$  is in fact made by piecewise constant functions on the curved mesh  $\gamma_{h,i}^c$ . By construction, both  $\mathbf{W}_{h,i}$  and  $Q_{h,i}$  are broken spaces, *i.e.*

$$\mathbf{W}_{h,i} = \mathbf{W}_{h,i1} \times \mathbf{W}_{h,i2} \quad \text{and} \quad Q_{h,i} = Q_{h,i1} \times Q_{h,i2},$$

where  $\mathbf{W}_{h,ij}$  is the restriction of  $\mathbf{W}_{h,i}$  on  $\gamma_{h,ij} = \mathcal{P}_i^{-1}(\gamma_{ij})$ , and we have that  $\mathbf{W}_{h,ij} \subset \mathbf{H}_{\text{div}}(\gamma_{h,ij})$ . Consequently, also  $\mathbf{W}_{h,i}^c$  and  $Q_{h,i}^c$  can be written as

$$\mathbf{W}_{h,i}^c = \mathbf{W}_{h,i1}^c \times \mathbf{w}_{h,i2}^c \quad \text{and} \quad Q_h^c = Q_{h,i1}^c \times Q_{h,i2}^c,$$

with  $\mathbf{W}_{h,ij}^c \subset \mathbf{W}_{ij}$  and  $Q_{h,ij}^c \subset Q_{ij}$ . Thus  $\mathbf{W}_{h,i}^c \subset \mathbf{W}_i$  and  $Q_{h,i}^c \subset Q_i$ . We define  $\mathbf{W}_h^c := \mathbf{W}_{h,1}^c \times \mathbf{W}_{h,2}^c$  and  $Q_h^c = Q_{h,1}^c \times Q_{h,2}^c \times \mathbb{R}$ , and analogously  $\mathbf{W}_h$  and  $Q_h$ . We can now write the discrete weak formulation of the coupled problem (16) and (17) as: find  $(\hat{\mathbf{u}}_h^c, \hat{p}_h^c) \in \mathbf{W}_h^c \times Q_h^c$  such that

$$\begin{cases} \mathcal{A}(\hat{\mathbf{u}}_h^c, \mathbf{w}_h^c) + \mathcal{B}(\hat{p}_h^c, \mathbf{w}_h^c) = \mathcal{F}(\mathbf{w}_h^c) & \forall \mathbf{w}_h^c \in \mathbf{W}_h^c \\ \mathcal{B}(q_h^c, \hat{\mathbf{u}}_h^c) = \mathcal{Q}(q_h^c) & \forall q_h^c \in Q_h^c. \end{cases} \quad (39)$$

We introduce the following weighted  $L^2$  norm on functions of  $L^2(\gamma_{h,i})$

$$\|w\|_{L_h^2(\gamma_{h,i})} = \int_{\gamma_{h,i}} (1 + \dot{D}^2)^{-1/2} w^2 d\gamma, \quad (40)$$

which, is equivalent to the natural  $L^2$  norm thanks to Lemma 5.1.

We define now the following problem on the polygonal lines approximating the fractures: find  $(\hat{\mathbf{u}}_h, \hat{p}_h) \in \mathbf{W}_h \times Q_h$  such that

$$\begin{cases} \mathcal{A}_h(\hat{\mathbf{u}}_h, \mathbf{w}_h) + \mathcal{B}_h(\hat{p}_h, \mathbf{w}_h) = \mathcal{F}_h(\mathbf{w}_h) & \forall \mathbf{w}_h \in \mathbf{W}_h \\ \mathcal{B}_h(q_h, \hat{\mathbf{u}}_h) = \mathcal{Q}_h(q_h) & \forall q_h \in Q_h, \end{cases} \quad (41)$$

where

$$\mathcal{A}_h(\mathbf{u}_h, \mathbf{w}_h) := \sum_{i=1}^2 a_{h,i}(\mathbf{u}_{h,i}, \mathbf{w}_{h,i}) + \sum_{\substack{i,j=1 \\ i \neq j}}^2 \eta_{ij}^I \left\{ \left\{ \mathbf{u}_{h,j} \cdot \boldsymbol{\tau}_{h,j} \right\}_{\hat{\mathbf{i}}_p} \right\} \left\{ \left\{ \mathbf{w}_{h,i} \cdot \boldsymbol{\tau}_{h,i} \right\}_{\hat{\mathbf{i}}_p} \right\}, \quad (42a)$$

$$\mathcal{B}_h(q_h, \mathbf{w}_h) := - \sum_{i=1}^2 (q_{h,i}, \nabla \boldsymbol{\tau}_{h,i} \cdot \mathbf{w}_{h,i})_{L^2(\gamma_{h,i})} + q_3 \llbracket \mathbf{w}_{h,i} \cdot \boldsymbol{\tau}_{h,i} \rrbracket_{\hat{\mathbf{i}}_p}, \quad (42b)$$

$$\mathcal{F}_h(\mathbf{w}) := \sum_{ij: \partial\gamma_{ij}^p \neq \emptyset} -\hat{g}_i \mathbf{w}_{h,i} \cdot \mathcal{P}_i^{-1} \mathbf{n}_D \quad (42c)$$

$$\mathcal{Q}_h(q) := \sum_{i=1}^2 - \left( \hat{f}_i \circ \mathcal{F}_i^{-1}, q_{h,i} \right)_{L_h^2(\gamma_i)} + \hat{f}_1 q_3. \quad (42d)$$

Here, the bilinear forms  $a_{h,i}$  are defined as

$$\begin{aligned} a_{h,i}(\mathbf{u}, \mathbf{w}) := & (\hat{\eta}_i \mathbf{u}, \mathbf{w})_{L_h^2(\gamma_i)} + \sum_{i=1}^2 \eta^I \frac{d_j}{d_i} \left( \hat{\xi}_0 \llbracket \mathbf{u}_{h,i} \cdot \boldsymbol{\tau}_{h,i} \rrbracket_{\hat{\mathbf{i}}_p} \llbracket \mathbf{w}_{h,i} \cdot \boldsymbol{\tau}_{h,i} \rrbracket_{\hat{\mathbf{i}}_p} + \right. \\ & \left. + \left\{ \left\{ \mathbf{u}_{h,i} \cdot \boldsymbol{\tau}_{h,i} \right\}_{\hat{\mathbf{i}}_p} \right\} \left\{ \left\{ \mathbf{w}_{h,i} \cdot \boldsymbol{\tau}_{h,i} \right\}_{\hat{\mathbf{i}}_p} \right\} \right) \quad \text{with } j \neq i. \end{aligned}$$

**Lemma 5.2** *Problem (39) is equivalent to (41) in the sense that if taken  $\hat{\mathbf{u}}_h = (\mathbf{u}_{h,1}, \mathbf{u}_{h,2}) \in \mathbf{W}_h$  and  $\hat{p}_h = (q_1, q_2, q_I) \in Q_h$  is a solution of (41) then the projections  $(\mathcal{P}_1 \mathbf{u}_{h,1}, \mathcal{P}_2 \mathbf{u}_{h,2}) \in \mathbf{W}_h^c$  and  $(\mathcal{P}_1 q_1, \mathcal{P}_2 q_2, q_I) \in Q_h^c$  are a solution of (39). Vice versa, if  $\hat{\mathbf{u}}_h^c = (\mathbf{u}_{h,1}^c, \mathbf{u}_{h,2}^c) \in \mathbf{W}_h^c$  and  $\hat{p}_h^c = (q_1^c, q_2^c, q_I) \in Q_h^c$  is a solution of (41) then  $(\mathcal{P}_1^{-1} \mathbf{u}_{h,1}^c, \mathcal{P}_2^{-1} \mathbf{u}_{h,2}^c) \in \mathbf{W}_h$  and  $(\mathcal{P}_1^{-1} q_1, \mathcal{P}_2^{-1} q_2, q_I) \in Q_h$  are a solution of (41).*

**Proof.** It is sufficient to apply the definition of the discrete spaces and of the transformations  $\mathcal{P}_i$  and  $\mathcal{P}_i^{-1}$ , together with (30), (40) and apply Lemma 5.1.  $\square$

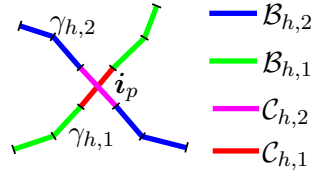


Figure 5: Subdivision of  $\gamma_{h,i} = \mathcal{C}_{h,i} \cup \mathcal{B}_{h,i}$ .

**Theorem 5.1 (Well posedness of the discrete problem)** *Under the same conditions of Theorem 4.1, problem (39) is well posed.*

**Proof.** We tackle problem (39) by considering the equivalent problem (41) instead. First of all we note that thanks to Lemma 5.1 all bilinear forms and functionals in (41) are bounded, since we have already demonstrated the boundedness of the ones used in (39). We now note that  $\mathbf{W}_{h,ij}$  does in fact define a one dimensional  $\mathbb{RT}_0$  finite element space on the “extended grid”  $\hat{\gamma}_{h,ij} = (\gamma_{h,ij} \setminus \mathcal{C}_{h,i}) \cup l_{i,j}^X$  and  $Q_{h,ij}$  a piecewise constant finite element space on  $\hat{\gamma}_{h,ij}$ . Therefore we can define a standard interpolation  $\Pi_{ij} : \mathbf{H}_{\text{div}}(\hat{\gamma}_{h,ij}) \rightarrow \mathbf{W}_{h,ij}$  and projection operators  $\pi_{ij} : L^2(\hat{\gamma}_{h,ij}) \rightarrow Q_{h,ij}$ . It is known that in one dimension the two operator commute with the tangential divergence, i.e.  $\nabla_{\tau_{h,i}} \cdot \Pi_{ij} \mathbf{v} = \pi_{ij} \nabla_{\tau_{h,i}} \mathbf{v}$ , for all  $\mathbf{v} \in \mathbf{H}_{\text{div}}(\hat{\gamma}_{h,ij})$ .

We can then repeat the same steps of Theorem 4.1 on problem (41), where now we take as velocity field associated to a given  $q_{h,ij} \in Q_{h,ij}$  the quantity  $\mathbf{v}_{h,ij} = \Pi_{ij} \nabla_{\tau_{h,i}} \phi_{ij}$  to prove the inf-sup stability of  $\mathcal{B}_h$ .  $\square$

**Theorem 5.2 (Maximum principle)** *The maximum principle is satisfied for problem (39) under the same conditions of Theorem 4.2.*

**Proof.** Again we refer first to the equivalent problem (41). In the absence of source term the second equation implies that  $\nabla_{\tau_{h,i}} \mathbf{u}_{h,i} = 0$  on each element of the extended grid  $\hat{\gamma}_{h,ij}$ . Therefore  $\mathbf{u}_{h,ij} = u_{h,ij} \boldsymbol{\tau}_{h,i}$  is constant. If for any couple  $i, j$  we take as test function  $\mathbf{w}_h$  the function such that  $\mathbf{w}_{h,ij} \cdot \boldsymbol{\tau}_{h,ij} = 1$  on all vertexes  $\mathbf{x}_k$  internal to  $\hat{\gamma}_{h,ij}$  and zero at all other nodes of  $\gamma_{h,1} \cup \gamma_{h,2}$  and on the intersection point  $\hat{\mathbf{i}}_p$ , then by simple computations, the first equation of (41) gives the following relation for the pressures  $\hat{p}_{h,ij,1}$  and  $\hat{p}_{h,ij,N_{ij}}$  at the first and last element  $l_{h,ij,1}$  and  $l_{h,ij,N_{ij}}$  of  $\hat{\gamma}_{h,ij}$ ,

$$\hat{p}_{h,ij,N_{ij}} - \hat{p}_{h,ij,1} = -\mathbf{u}_{h,ij} \int_{\hat{\gamma}_{h,ij}} \hat{\eta}_i \mathbf{w}_{h,ij} \cdot \boldsymbol{\tau}_{h,ij} dx.$$

Since  $\mathbf{w}_{h,ij} \cdot \boldsymbol{\tau}_{h,ij}$  is not negative,  $\hat{p}_{h,ij}$  is thus varying monotonically at the interior nodes of  $\hat{\gamma}_{h,ij}$ . Thus, also in this case we are left to prove the same conditions (a) and (b) stated in Theorem 4.2, where now  $\mathbf{g} = [\hat{p}_{h,11,1}, \hat{p}_{h,12,1}, \hat{p}_{h,21,1}, \hat{p}_{h,2,1}]^\top$  and  $\mathbf{p} = [\hat{p}_{h,11,N_h}, \hat{p}_{h,12,N_h}, \hat{p}_{h,21,N_h}, \hat{p}_{h,22,N_h}]^\top$ . Since the interface conditions at the intersection are unchanged from the continuous case we can repeat the same argument of the cited theorem to conclude the proof for the solution of (41).

As for the solution of (39), it is sufficient to recall Lemma 5.2 and note that the elemental values of the pressure are unchanged in the two problems and that the transformation  $\mathcal{P}_i$  maintains monotonicity.  $\square$

**Theorem 5.3 (Convergence)** *Let  $(\hat{\mathbf{u}}, \hat{p})$  solution of (18) with  $\hat{\mathbf{u}}_i \in \mathbf{H}^2(\gamma_i)$  and  $\hat{p}_i \in H^1(\gamma_i)$  and  $(\hat{\mathbf{u}}_h^c, \hat{p}_h^c)$  solution of (39), then*

$$\|\hat{\mathbf{u}} - \hat{\mathbf{u}}_h^c\|_{\mathbf{W}} + \|\hat{p} - \hat{p}_h^c\|_Q \leq Ch (|\hat{\mathbf{u}}|_{\mathbf{W}} + |\hat{p}|_Q),$$

where

$$|\hat{\mathbf{u}}|_{\mathbf{W}}^2 = \sum_{i=1}^2 \sum_{l_{h,i}^c \in \gamma_{h,i}^c} |\nabla_{\boldsymbol{\tau}_i} \cdot \hat{\mathbf{u}}|_{\mathbf{H}^1(l_{h,i}^c)}^2 \quad \text{and} \quad |\hat{p}|_Q^2 = \sum_{i=1}^2 |\hat{p}|_{H^1(\gamma_i)}^2.$$

**Proof.** By standard results of saddle point problems [6, 8] we have that there exist a constant  $C$  independent from  $h$  such that

$$\|\hat{\mathbf{u}} - \hat{\mathbf{u}}_h^c\|_{\mathbf{W}} + \|\hat{p} - \hat{p}_h^c\|_Q \lesssim \left( \inf_{\mathbf{w}_h^c \in \mathbf{W}_h^c} \|\hat{\mathbf{u}} - \mathbf{w}_h^c\|_{\mathbf{W}} + \inf_{q_h^c \in Q_h^c} \|\hat{p} - q_h^c\|_Q \right).$$

We set  $\mathcal{P}$  to be the composition of the operators  $\mathcal{P}_i$ , and operating on each portion of  $\gamma_{ij}$  of the fractures. That is, for a  $\mathbf{w}_h^c \in \mathbf{W}$  we have that  $\mathcal{P}\mathbf{w}_h^c = \prod_{i,j=1}^2 \mathcal{P}_i \mathbf{w}_{i,j}^c \in \mathbf{W}_h$ . Because of Lemma 5.1 we have

$$\|\hat{\mathbf{u}} - \mathbf{w}_h^c\|_{\mathbf{W}} \lesssim \|\mathcal{P}^{-1}\hat{\mathbf{u}} - \mathbf{w}_h\|_{\mathbf{W}_h},$$

where  $\mathbf{w}_h = \mathcal{P}^{-1}\mathbf{w}_h^c \in \mathbf{W}_h$ . We choose then on each  $\gamma_{h,i}$ ,  $\mathbf{w}_{h,i} = \Pi_i^* \mathcal{P}^{-1}\hat{\mathbf{u}}_i$ , where  $\Pi_i^*$  is the extended  $\mathbb{RT}_0$  interpolant for the velocity field on described in [7], which is an extension of that introduced in [5]. We can then apply the interpolation error bound contained in the cited references with the results of Lemma 5.1 to obtain

$$\|\mathcal{P}^{-1}\hat{\mathbf{u}} - \mathbf{w}_h\|_{\mathbf{W}_h} \lesssim \sum_{i=1}^2 \sum_{l_{h,i} \in \gamma_{h,i}} |l_{h,i}| |\nabla_{\boldsymbol{\tau}_{h,i}} \cdot \mathcal{P}^{-1}\hat{\mathbf{u}}|_{\mathbf{H}^1(l_{h,i})}.$$

Applying (31) and using the fact that  $\|\nabla_{\boldsymbol{\tau}_i} \cdot \hat{\mathbf{u}}\|_{L^2(l_{h,i}^c)}$  is bounded we obtain

$$\inf_{\mathbf{w}_h^c \in \mathbf{W}_h^c} \|\hat{\mathbf{u}} - \mathbf{w}_h^c\|_{\mathbf{W}} \lesssim h |\hat{\mathbf{u}}|_{\mathbf{W}}.$$

We proceed analogously for the pressure term. We consider the transformation  $\mathcal{P}$  which maps  $(q_{11}, q_{12}, q_{21}, q_{22}, q_I) \in Q_h$  to  $(\mathcal{P}_1 q_{11}, \mathcal{P}_1 q_{12}, \mathcal{P}_2 q_{21}, \mathcal{P}_2 q_{22}, q_I) \in Q_h^c$ . We have thanks to Lemma 5.1

$$\|\hat{p} - q_h^c\|_Q \lesssim \|\mathcal{P}^{-1}\hat{p} - q_h\|_{Q_h}.$$



We choose  $q_h = (q_{h,11}, q_{h,12}, q_{h,21}, q_{h,22}, q_{h,I})$  by applying the extended  $L^2$  interpolant  $\pi_i^*$  defined in [7] on  $(\mathcal{P}_i^{-1}q_{i1}, \mathcal{P}_i^{-1}q_{i2})$ , for  $i = 1, 2$ , while we set  $q_{h,I} = q_I$ . Using the result of the interpolation error for this extended interpolant we have

$$\|\mathcal{P}^{-1}\hat{p} - q_h\|_{Q_h} \lesssim \sum_{i=1}^2 \sum_{l_{h,i} \in \gamma_{h,i}} |l_{h,i}| |\mathcal{P}_i^{-1}\hat{p}|_{H^1(\gamma_{h,i})}.$$

We then apply (37) on each  $\gamma_{h,ij}$  to map back on the curve  $\gamma_{ij}$  and obtain the wanted result.  $\square$

**Remark 4** *In the numerical setting we will solve the problem in the form given by (41). Note that, since we use  $\mathbb{RT}_0$  finite elements we may replace the norm  $L_h^2(\gamma_{h,i})$  with the (simpler to compute) norm  $L^2(\gamma_{h,i})$ . Indeed, since  $\dot{D} = \mathcal{O}(h)$  by the application of the Strang Lemma to our problem we obtain a solution converging with the same order of convergence.*

## 6 Applicative examples

We present some numerical experiments to validate the proposed reduced model and verify the theoretical results.

### 6.1 Model error

We start with an analysis to validate the reduced model presented in Section 3. We consider two rectilinear fractures  $\gamma_1$  and  $\gamma_2$  of thickness  $d_i = 0.005$  intersecting orthogonally. The fracture permeabilities are  $K_{1,\tau} = 1$  and  $K_{2,\tau} = 10^{-2}$ , respectively and in the intersection we have  $\mathbf{K}_I = 10^{-2}\mathbf{I}$ . Thus,  $\gamma_2$  acts as a barrier for the other fracture. The scalar source term is set to zero in both fractures and the shape parameter is taken as  $\hat{\xi}_0 = 0.25$ . We impose only essential boundary conditions, namely  $g_{1,1} = 0$ ,  $g_{1,2} = 1$ ,  $g_{2,1} = -1$  and  $g_{2,2} = 1$ . We want to compare the results obtained with the reduced model with a reference solution obtained solving the complete two-dimensional problem with a very fine two-dimensional grid of approximately  $120 \cdot 10^3$  triangular elements.

We compare our reduced model with that proposed in [1, 3], where continuity of pressure is assumed at the interface. The results are represented in Figure 6. The solution of the two-dimensional problem is smooth in the intersection region but nevertheless exhibits a steep pressure gradient due to the low permeability imposed in  $\Omega_2$  and in the intersection region. If we consider the reduced model with the coupling conditions presented in [1, 3] the solution cannot not reproduce this behaviour, while with the proposed conditions (17) we are able to replace the pressure gradient of the 2D solution with a correct pressure jump at the intersection and thus obtain the correct pressure gradient and flux in each branch of the fractures.

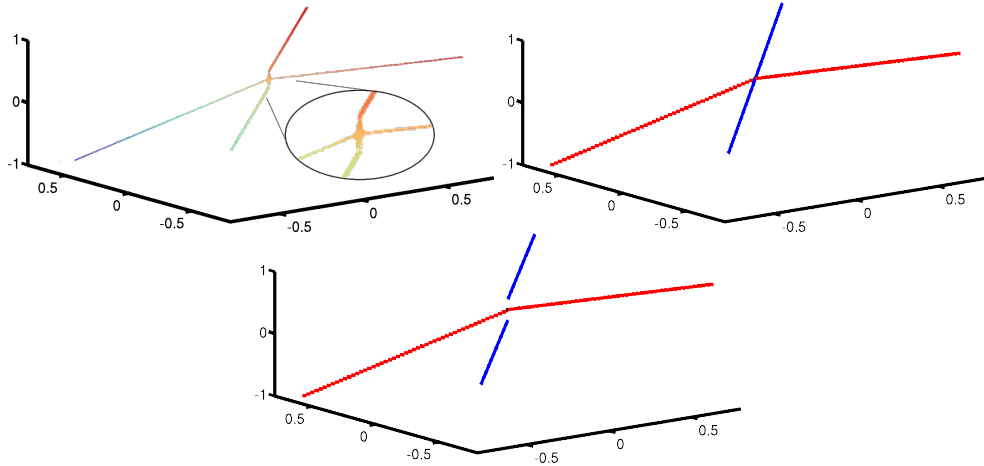


Figure 6: In the top-left figure  $p$  and a zoom near the intersection of (3) with (4). In the top-right figure the solution of (16) with the conditions of [1, 3]. At the bottom the solution (16) with (17). In the 1D simulations  $\gamma_1$  is coloured in blue and  $\gamma_2$  in red.

We now consider the behaviour of our reduced model for different values of the parameters. To this purpose we compare the pressure of the fractures at the intersection point and the pressure in the intersection obtained solving the original problem (3), (4) with the reduced pressures given by (7),(8). The solution of the two-dimensional problem is computed again with a fine grid and the computed pressure is averaged in the intersection region and on each edge of  $I$  to obtain the values to compare with those produced by the reduced model.

Table 1: Comparison of the model error for different values of the slope  $m$ . The two-dimensional mesh is formed by  $\sim 120k$  triangles, while both the mono-dimensional meshes have  $\sim 50$  segments.

	$ m  = 1$			$ m  = 10$			$ m  = 0.1$		
	2D	1D	$err_{rel}$	2D	1D	$err_{rel}$	2D	1D	$err_{rel}$
$p_I$	0.494	0.493	0.2%	0.495	0.493	0.4%	0.495	0.493	0.4%
$\hat{p}_{1,1}$	0.366	0.327	10.7%	0.324	0.331	2.2%	0.314	0.324	3.2%
$\hat{p}_{1,2}$	0.624	0.663	6.25%	0.666	0.660	0.9%	0.676	0.666	1.2%
$\hat{p}_{2,1}$	0.492	0.478	2.85%	0.639	0.642	0.5%	0.337	0.317	5.9%
$\hat{p}_{2,2}$	0.496	0.498	0.4%	0.351	0.334	4.8%	0.652	0.658	0.9%

We first consider the effect of the intersection angle. Let the two fractures have slope  $\pm m$  respectively in the  $xy$  plane. We set  $K_{1,\tau} = 1$ ,  $K_{2,\tau} = 10^{-2}$ ,  $\mathbf{K}_I = 10^{-2}\mathbf{I}$  and  $d_i = 10^{-2}$ . Table 1 shows the comparison of the pressures for different values of  $m$ . The relative error  $err_{rel}$  is computed as the ratio between the difference of the corresponding pressures and the pressure of the bi-dimensional grid. We can see that the errors are rather small and independent on  $m$ . This indicates that reduced model is sound and capable of treating reasonable

well intersections at different angle.

Table 2: Comparison of the model error for decreasing values of the thickness  $d_i$ . The spacing of the meshes are the same as in Table 1.

	$d_i = 0.01$			$d_i = 0.005$			$d_i = 0.0025$		
	$2D$	$1D$	$err_{rel}$	$2D$	$1D$	$err_{rel}$	$2D$	$1D$	$err_{rel}$
$p_I$	0.495	0.494	0.2%	0.495	0.494	0.2%	0.495	0.495	-
$\hat{p}_{1,1}$	0.411	0.392	4.6%	0.45	0.437	2.9%	0.472	0.463	1.9%
$\hat{p}_{1,2}$	0.579	0.598	3.3%	0.54	0.553	2.4%	0.519	0.527	1.5%
$\hat{p}_{2,1}$	0.493	0.483	2%	0.494	0.485	1.8%	0.495	0.486	1.8%
$\hat{p}_{2,2}$	0.495	0.498	0.6%	0.495	0.498	0.6%	0.495	0.498	0.6%

Table 2 shows instead the relative errors when the thickness of the fractures decreases. In this case we have taken  $\mathbf{K}_I = 50.5^{-1}\mathbf{I}$ , *i.e.* the harmonic mean of the  $K_{i,\tau}$ , and  $|m| = 1$ . Also in this case the errors are rather small and, as we expected, they decrease when the thicknesses decrease. Even if this is not a rigorous analysis of the model error, it gives numerical evidence of its asymptotic behaviour with respect to the fracture thickness.

Finally we address some different choices to prescribe the permeability in the intersection region. The choice should of course be driven by physical arguments. For instance, if we assume that  $\gamma_1$  is “younger” than  $\gamma_2$ , *i.e.* it was generated after  $\gamma_2$ , than  $\mathbf{K}_I$  should be equal to the  $K_{1,\tau}$ . Alternatively we can impose a tensor  $\mathbf{K}_H = K_H\mathbf{I}$  that is the harmonic mean of  $K_{i,\tau}$ , if we suppose that the properties of each  $\gamma_i$  are mixed in  $I$ . Finally we can impose to  $\mathbf{K}_I$ , in the direction aligned to each  $\gamma_i$ , the value  $K_{i,\tau}$  obtaining a non-isotropic tensor  $\mathbf{K}_T$ . In Table 3 we compare the three choices for a system of two orthogonal fractures of thickness  $d_i = 0.01$  and permeabilities  $K_{1,\tau} = 1$ ,  $K_{2,\tau} = 10^{-4}$ . This test is the most critical for our reduced model. The best fit between the two dimensional and our reduced model is obtained with the third strategy, imposing a non-isotropic tensor at the intersection. In the other cases, the mismatch of the pressure, particularly evident for  $\hat{p}_{1,1}$ , is due to the complex two-dimensional pressure distribution in the intersection region  $I$  that the reduced model is not able to reproduce in full.

Table 3: Comparison of the model error for different values of  $\mathbf{K}_I$ . The spacing of the meshes are the same as in Table 1.

	$\mathbf{K}_I = K_{2,\tau}\mathbf{I}$			$\mathbf{K}_I = \mathbf{K}_H$			$\mathbf{K}_I = \mathbf{K}_T$		
	$2D$	$1D$	$err_{rel}$	$2D$	$1D$	$err_{rel}$	$2D$	$1D$	$err_{rel}$
$p_I$	0.499	0.497	0.4%	0.500	0.499	0.2%	0.500	0.500	-
$\hat{p}_{1,1}$	0.0208	0.01	51.9%	0.029	0.019	34.5%	0.502	0.505	0.6%
$\hat{p}_{1,2}$	0.979	0.990	1.1%	0.971	0.981	1.1%	0.500	0.485	3%
$\hat{p}_{2,1}$	0.497	0.483	2.9%	0.498	0.488	2%	0.500	0.505	1%
$\hat{p}_{2,2}$	0.500	0.5024	0.5%	0.500	0.502	0.5%	0.500	0.505	1%

## 6.2 Maximum principle

We want to verify, with numerical experiments, the bounds derived in Theorem 5.2 for the parameter  $\hat{\xi}_0$  that ensure the fulfilment of the maximum principle. Let us consider two fractures of the same length  $L = 1$  and thickness  $d_i = 0.01$  that intersect orthogonally. We set  $\eta_i = 1$  while in the intersection point we consider an isotropic permeability tensor  $\mathbf{K}_I = 10^{-4}\mathbf{I}$ . We impose pressure as a boundary condition on all four end points, in particular we set  $g_{i,1} = 0$  and  $g_{i,2} = 1$  for  $i = 1, 2$ . For this configuration, according to Theorem 5.2, the maximum principle is satisfied if  $\hat{\xi}_0 \geq 1/8$ . Figure 7 shows the solution we obtained with  $\hat{\xi}_0 = 0$ , a value that does not satisfy the hypotheses: it is clear that the maximum principle is violated, indeed the pressure inside the domain exceeds 1 which is the maximum at the boundary. In the same figure we represent the solution obtained with  $\hat{\xi}_0 = 1/8$ , which satisfies the maximum principle, as indicated by the theory.

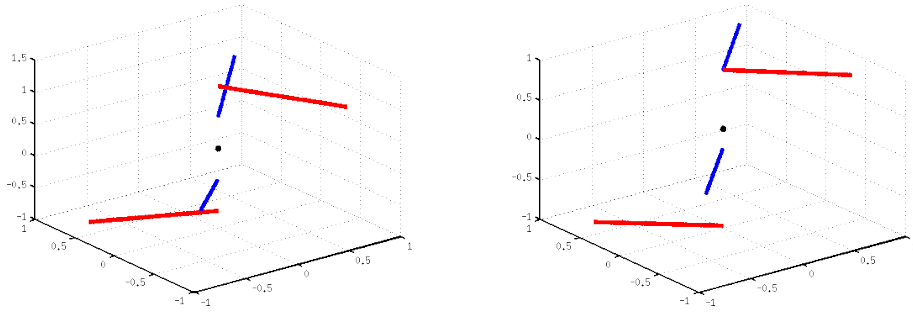


Figure 7: In the left image  $\hat{\xi}_0$  is such that the maximum principle is not fulfilled, while in the right is fulfilled.

In the first part of Table 4 we report the maximum value of pressure in the domain for different  $\hat{\xi}_0$  to prove that the violation of the maximum principle vanishes as we approach the theoretical bounds.

Table 4: Top values of  $\max_i \hat{p}_i$  for different  $\hat{\xi}_0$  in the orthogonal case, bottom for the non-orthogonal case.

$\hat{\xi}_0$	0.025	0.05	0.075	0.1	0.125
$\max_i \hat{p}_i$	1.022	1.003	0.996	0.992	0.990
$\hat{\xi}_0$	0	0.0025	0.005	0.0075	0.01
$\max_i \hat{p}_i$	1.116	1.033	0.993	1.018	1.035

We then consider two fractures that intersect forming a small angle of  $0.2rad$ . In this case the bound on  $\hat{\xi}_0$  are  $4.934 \cdot 10^{-3} \leq \hat{\xi}_0 \leq 5.034 \cdot 10^{-3}$ . We report in the second part of Table 4 the maximum pressure in the domain for different  $\hat{\xi}_0$ : it can be observed that 0.005 is indeed the only value for which the solution fulfils the maximum principle. This numerical experiment points out the bounds are

rather sharp.

### 6.3 Convergence rates

Let us consider two intersecting fractures described by equations

$$\gamma_1 = \{(x, y) : y = x\} \quad \text{and} \quad \gamma_2 = \{(x, y) : y = 1 - x\}, \quad x \in \left[-\frac{\sqrt{2}}{2}, \frac{\sqrt{2}}{2}\right].$$

The permeability of the fractures is  $K_{i,\tau} = 1$  while  $\mathbf{K}_I = 0.01\mathbf{I}$ . Both fractures have thickness  $d_i = 0.01$ , the boundary conditions are  $\mathbf{g} = [0, 1, 0, 1]$  and the source term is set to  $f_1 = 0.01$  only in  $\gamma_1$  for  $x < 0$ . Finally choosing  $\xi_0 = \frac{1}{4}$ , the exact solution is

$$\hat{p}_1(s) = \begin{cases} -\frac{s^2}{2} + \frac{13}{12}s & s \in [0, 1) \\ -\frac{1}{4}(1-s) + 1 & s \in (1, 2] \end{cases}, \quad \hat{p}_2(s) = \begin{cases} \frac{5}{12}s & s \in [0, 1) \\ -\frac{1}{4}(1-s) + 1 & s \in (1, 2] \end{cases}$$

and  $\hat{p}_I = 5/8$ . Figure 8 shows the errors computed with decreasing grid spacings. The numerical results are in good agreement with theorem 5.3.

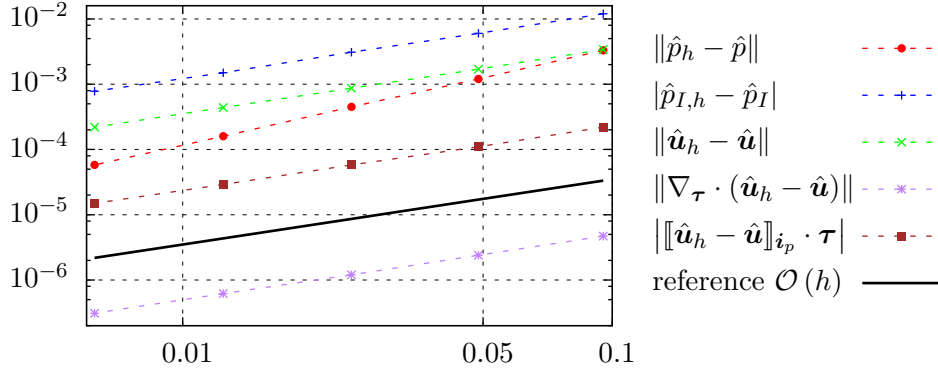


Figure 8: Convergence rates for each pieces of the norm  $\mathbf{W}$  and  $Q$ . In the legend we have indicated by  $\|\cdot\|$  the  $L^2$  norm.

Let us now consider the case of curved fractures to evaluate the error associated with the approximation of geometry as piecewise linear. The two fractures are now described by the following equations

$$\gamma_1 = \{(x, y) : x = 0, y = \theta\} \quad \text{and} \\ \gamma_2 = \{(x, y) : x = \sin \theta, y = 1 + \cos \theta\}, \quad \theta \in [-1, 1].$$

We impose the same permeabilities, thicknesses, source term and boundary conditions as in the previous case: since the arc length of the four branches is the same we obtain the same exact solution. The errors obtained for different grid spacings are reported in Figure 9. It can be observed that the error decreases

linearly as in the case of straight fractures and the absolute values are comparable, thus, if the grid size is small enough compared to the fracture curvature, the approximation of geometry does not affect the quality of the numerical solution.

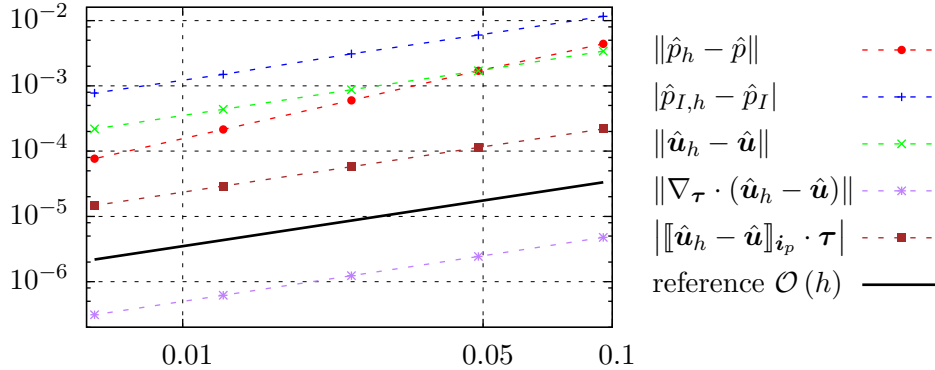


Figure 9: Convergence rates for the curve case.

#### 6.4 Network of fractures

As already mentioned the method proposed in this paper can be applied to networks composed by an arbitrary number of fractures. Let us consider a set of three fractures  $\gamma_{1,2,3}$  characterized by the same permeability. Imposing  $g_{i,1} = 0$  and  $g_{i,2} = 1$  for all  $i$  we obtain the pressure distribution reported in Figure 10. We now insert a new fracture  $\gamma_4$  with lower permeability, and, following the considerations of subsection 6.1, we impose in all the intersection with  $\gamma_4$  the permeability of this latter. As shown in Figure 10 the solution obtained with the classical model [1, 3] is everywhere continuous while the new coupling conditions allow us to mimic the blocking nature of  $\gamma_4$ .

In realistic applications fractured porous media are often characterized by the density and orientation of the fractures rather than by detailed information on the geometry and properties of the single fracture. In this second test case we consider a grid of  $N_H$  horizontal fractures and  $N_V$  fractures that form a variable angle  $\theta$  with the horizontal ones. We impose homogeneous boundary conditions for the pressure on all tips except for one where we set  $g_{1,2} = 1$  as shown in Figure 11 left. Figure 11 right shows the resulting pressure field for  $N_H = N_V = 5$  and  $\theta = 80^\circ$ . Thanks to the efficiency of the reduced one-dimensional model we are able to analyse different configuration with a low computational cost. Figure 12 shows the value of the pressure in the centre of the network for different orientations of the fractures, *i.e.* different angles  $\theta$ , and for increasing density of the vertical fractures in the orthogonal case. We can observe that as we increase the number of fractures, thus the transmissibility of the network, the pressure in the central point tends to an asymptotic value.

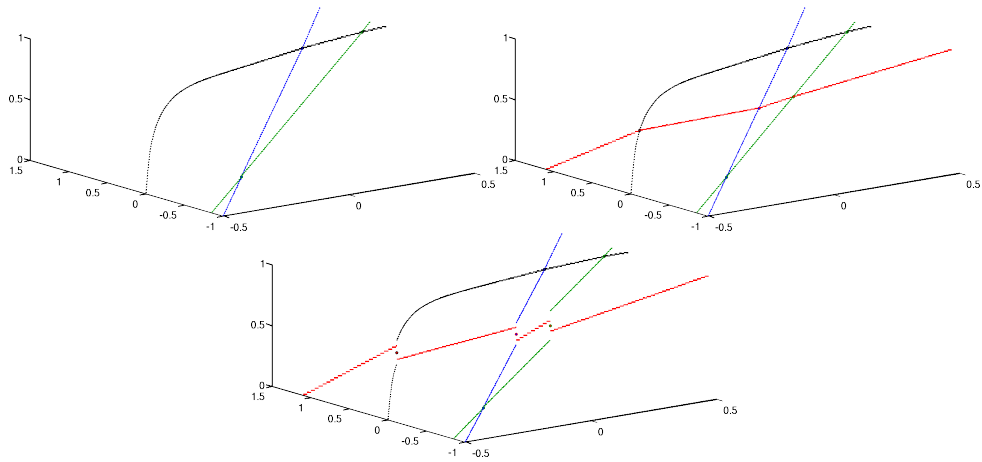


Figure 10: Top-left:  $\hat{p}_i$  without  $\gamma_4$ . Top-right and bottom:  $\hat{p}_i$  with the classical conditions and our model respectively.

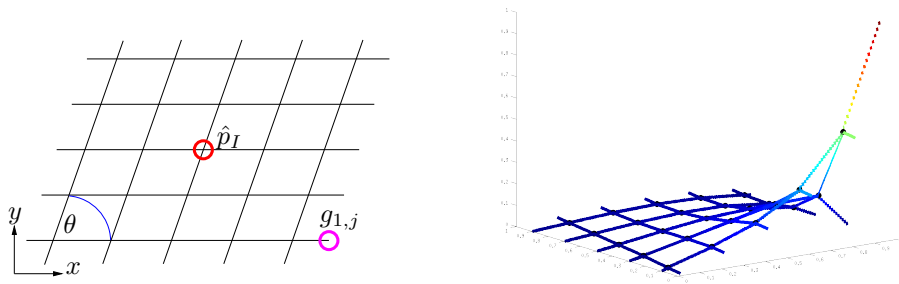


Figure 11: Left grid of fractures with the interesting point. Right simulation of ten fractures with  $\theta = 80^\circ$ .

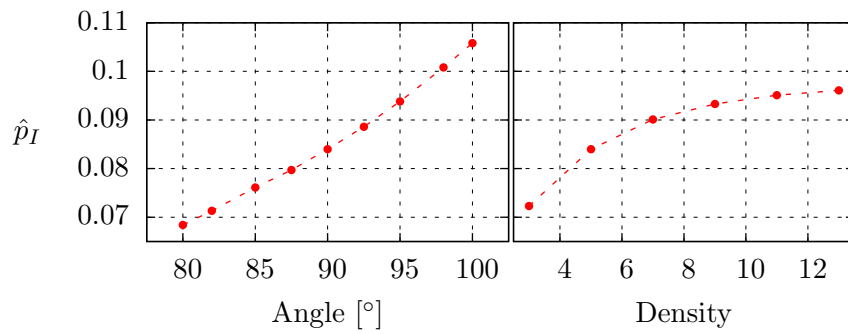


Figure 12: In the left  $\hat{p}_I$  for different values of the angle between the fractures. In the right  $\hat{p}_I$  increasing the number of the fractures.

## 7 Conclusions

In this paper we derived and analysed a reduced model for flow in a network of fractures. The derivation is similar to that given in [15] and [7], yet here we propose new coupling conditions to handle in a more realistic way the intersecting fractures. These conditions take into account the intersection angle and, by allowing a discontinuous pressure at the interface they are capable of giving accurate results also in the case where the permeability of the fractures are very different. This is not the case for the coupling conditions in [3, 2]. This can be relevant to applications since a fracture may sometimes act as a barrier or a preferential path.

Well posedness analysis has been given for both the continuous and discrete problem and numerical experiments have been performed to validate the theoretical results of convergence and positivity. The comparison with two dimensional simulations on refined grids proved that the new coupling conditions give reasonable accurate results, and they perform better than the classical one in the case of impermeable fractures. We have also shown how the model can be used to simulate more realistic configurations with the presence of several intersecting fractures.

Further developments will consist in extending the analysis to the coupling between the network and the surrounding porous medium introduced in [9], to obtain a complete framework for the simulation of mono-phase flow in presence of an arbitrary set of fractures.

We have dealt only with two dimensional problems. However the derivation here presented forms the basis for a similar reduced model in a three dimensional setting. The main difficulty in the extension to three dimensional problems is that the interface condition is not anymore an algebraic one, but it involves the interaction with a one-dimensional model that describes the flow along the intersection. This matter is the subject of ongoing work. Two dimensional simulations have however, already an applicative relevance. They may be used to better understand the behaviour of the flow in the presence of fractures and drive, for instance, upscaling techniques.

## Acknowledgement

This work has been supported by ENI s.p.a. The first and third authors also acknowledge the support of MIUR through the PRIN09 project n. 2009Y4RC3B 001.

## References

- [1] C. ALBOIN, J. JAFFRÉ, J. ROBERTS, AND C. SERRES, *Modeling fractures as interfaces for flow and transport in porous media*, in Fluid flow and



transport in porous media: mathematical and numerical treatment (South Hadley, MA, 2001), Z. Chen and R. Ewing, eds., vol. 295 of *Contemp. Math.*, Amer. Math. Soc., Providence, RI, 2002, pp. 13–24.

- [2] C. ALBOIN, J. JAFFRÉ, J. ROBERTS, X. WANG, AND C. SERRES, *Domain decomposition for some transmission problems in flow in porous media*, vol. 552 of *Lecture Notes in Phys.*, Springer, Berlin, 2000, pp. 22–34.
- [3] L. AMIR, M. KERN, V. MARTIN, AND J. ROBERTS, *Décomposition de domaine et préconditionnement pour un modèle 3D en milieu poreux fracturé*, in *Proceeding of JANO 8*, 8th conference on Numerical Analysis and Optimization, December 2005.
- [4] P. ANGOT, F. BOYER, AND F. HUBERT, *Asymptotic and numerical modelling of flows in fractured porous media*, *M2AN Math. Model. Numer. Anal.*, 43 (2009), pp. 239–275.
- [5] R. BECKER, E. BURMAN, AND P. HANSBO, *A Nitsche extended finite element method for incompressible elasticity with discontinuous modulus of elasticity*, *Comput. Methods Appl. Mech. Engrg.*, 198 (2009), pp. 3352–3360.
- [6] F. BREZZI AND M. FORTIN, *Mixed and hybrid finite element methods*, vol. 15 of *Computational Mathematics*, Springer Verlag, Berlin, 1991.
- [7] C. D’ANGELO AND A. SCOTTI, *A mixed finite element method for Darcy flow in fractured porous media with non-matching grids*, *ESAIM Math. Model. Numer. Anal.*, (2011).
- [8] A. ERN AND J. GUERMOND, *Theory and practice of finite elements*, Applied mathematical sciences, Springer, 2004.
- [9] A. FUMAGALLI, *Numerical modelling of flows in fractured porous media by the XFEM method*, PhD thesis, Politecnico di Milano, 2012.
- [10] A. FUMAGALLI AND A. SCOTTI, *A reduced model for flow and transport in fractured porous media with non-matching grids*, in *ENUMATH 2011 Proceedings*, Springer, 2012. Accepted.
- [11] ———, *An unfitted method for two-phase flow in fractured porous media*, in *CMWR 2012 Proceedings*, 2012. Submitted.
- [12] A. HANSBO AND P. HANSBO, *A finite element method for the simulation of strong and weak discontinuities in solid mechanics*, *Comput. Methods Appl. Mech. Engrg.*, 193 (2004), pp. 3523–3540.
- [13] J. JAFFRÉ, V. MARTIN, AND J. ROBERTS, *Generalized cell-centered finite volume methods for flow in porous media with faults*, in *Finite volumes for*

complex applications, III (Porquerolles, 2002), Hermes Sci. Publ., Paris, 2002, pp. 343–350.

- [14] J. JAFFRÉ, M. MNEJJA, AND J. ROBERTS, *A discrete fracture model for two-phase flow with matrix-fracture interaction*, *Procedia Computer Science*, 4 (2011), pp. 967–973.
- [15] V. MARTIN, J. JAFFRÉ, AND J. ROBERTS, *Modeling fractures and barriers as interfaces for flow in porous media*, *SIAM J. Sci. Comput.*, 26 (2005), pp. 1667–1691.
- [16] A. QUARTERONI AND A. VALLI, *Numerical approximation of partial differential equations*, vol. 23 of Springer Series in Computational Mathematics, Springer-Verlag, Berlin, 1994.

# MOX Technical Reports, last issues

Dipartimento di Matematica “F. Brioschi”,  
Politecnico di Milano, Via Bonardi 9 - 20133 Milano (Italy)

- 31/2012** BONIZZONI, F.; BUFFA, A.; NOBILE, F:  
*Moment equations for the mixed formulation of the Hodge Laplacian with stochastic data*
- 32/2012** FORMAGGIA, L.; FUMAGALLI, A.; SCOTTI A.; RUFFO, P  
*A reduced model for Darcy s problem in networks of fractures*  
BONIZZONI, F.; BUFFA, A.; NOBILE, F.  
*Moment equations for the mixed formulation of the Hodge Laplacian with stochastic data*
- 30/2012** BECK, J.; NOBILE, F.; TAMELLINI, L.; TEMPONE, R.;  
*Convergence of quasi-optimal Stochastic Galerkin Methods for a class of PDES with random coefficients*
- 29/2012** CHEN, P.; QUARTERONI, A.; ROZZA, G.  
*Stochastic Optimal Robin Boundary Control Problems of Advection-Dominated Elliptic Equations*
- 28/2012** CANUTO, C.; NOCHETTO, R.H.; VERANI, M.  
*Contraction and optimality properties of adaptive Legendre-Galerkin methods: the 1-dimensional case*
- 27/2012** FIGOLI, D.; SECCHI,P.  
*Estimation of the mean for spatially dependent data belonging to a Riemannian manifold*
- 26/2012** TAMELLINI, L.; LE MAITRE, O.; NOUY, A.  
*Model reduction based on Proper Generalized Decomposition for the Stochastic steady incompressible Navier-Stokes equations*
- 25/2012** MANFREDINI, F.; PUCCI, P.; SECCHI, P.; TAGLIOLATO, P.; VANTINI, S.; VITELLI, V.  
*Treelet decomposition of mobile phone data for deriving city usage and mobility pattern in the Milan urban region*
- 24/2012** ANTONIETTI, P.F.; GIANI, S.; HOUSTON, P.  
*hpVersion Composite Discontinuous Galerkin Methods for Elliptic Problems on Complicated Domains*